Published in final edited form as:

Nature. 2021 March ; 591(7849): 275–280. doi:10.1038/s41586-020-03151-1.

STING controls nociception via type-I interferon signaling in sensory neurons

Christopher R. Donnelly[1], **Changyu Jiang**[1], **Amanda S. Andriessen**[1], **Kaiyuan Wang**[1], **Zilong Wang**[1], **Huiping Ding**[6], **Junli Zhao**[1], **Xin Luo**[1], **Michael S. Lee**[1], **Yu L. Lei**[4,5], **William Maixner**[1], **Mei-Chuan Ko**[6,7], **Ru-Rong Ji**[1,2,3]

[1]Center for Translational Pain Medicine, Department of Anesthesiology, Duke University Medical Center, Durham, North Carolina, USA

[2]Department of Neurobiology, Duke University Medical Center, Durham, North Carolina, USA

[3]Department of Cell Biology, Duke University Medical Center, Durham, North Carolina, USA

[4]Department of Periodontics and Oral Medicine, University of Michigan, Ann Arbor, Michigan, USA.

[5]University of Michigan Rogel Cancer Center, Ann Arbor, Michigan, USA.

[6]Department of Physiology and Pharmacology, Wake Forest School of Medicine, Winston-Salem, North Carolina, NC 27157, USA

[7]W.G. Hefner Veterans Affairs Medical Center, Salisbury, North Carolina, NC 28144

Abstract

The innate immune regulator STING is a critical sensor of self- and pathogen-derived DNA, leading to the induction of type-I interferons (IFN-I) and other cytokines which promote immune cell-mediated eradication of pathogens and neoplastic cells [1,2]. STING has also emerged as a robust driver of antitumor immunity, leading STING activators and small molecule agonists to be developed as cancer immunotherapy adjuvants [3]. Pain, transmitted by peripheral nociceptive sensory neurons (nociceptors), also aids in host defense by alerting organisms to the presence of potentially damaging stimuli, including pathogens and cancer cells [4,5]. Here, we demonstrate that STING is a critical regulator of nociception through IFN-I signaling in peripheral nociceptors. We show that mice lacking STING or IFN-I signaling exhibit hypersensitivity to nociceptive stimuli and heightened nociceptor excitability. Conversely, intrathecal activation of STING produces robust antinociception in mice and non-human primates (NHPs). STING-mediated antinociception is governed by IFN-Is, which rapidly suppress excitability of mouse, NHP, and human nociceptors.

Correspondence and requests for materials should be addressed to Ru-Rong Ji (ru-rong.ji@duke.edu) and Christopher R. Donnelly (christopher.donnelly@duke.edu).

Author contributions

C.R.D. and R.R.J. conceived and shaped the overall direction of the project. C.R.D., C.J., K.W., A.S.A., Z.W., J.Z., X.L., and M.S.L. performed experiments. H.D. performed behavioral testing in non-human primates under the guidance of M.C.K. Y.L.L. and W.M. contributed to the experimental design. C.R.D. and R.R.J. wrote the manuscript with feedback and discussions from all co-authors.

Competing interests

R.R.J. is a consultant of Boston Scientific and received research support from the company. This activity is not related to this study. C.R.D. and R.R.J. also filed a patent, “Treatment of neuropathic and cancer pain using agonists of stimulator of interferon response cGAMP interactor-1 (STING1)” in association with Duke University. The other authors declare no competing interests.

Our findings establish the STING/IFN-I signaling axis as a critical regulator of physiological nociception and a promising new target for treating chronic pain.

Introduction

Nociception, or the detection of noxious stimuli, is a highly evolutionarily conserved system [6]. Although peripheral nociceptors were classically thought to serve as simple sensors of hazardous stimuli, present to elicit withdrawal and future avoidance of pain-evoking stimuli, nociceptors are now recognized as critical regulators of inflammation and immunity [7,8]. Nociceptors can be directly activated by damage- or pathogen-associated molecular patterns (DAMPs or PAMPs) produced by invading pathogens or damaged host cells, evoking pain, itch, or analgesia [5]. Deep sequencing of dorsal root ganglion (DRG) sensory neurons demonstrates that nociceptors express a large array of DAMP or PAMP-sensing pattern recognition receptors (PRRs) canonically expressed by immune cells and associated with host defense [5,9]. We observed that STING (recently renamed STING1, or stimulator of interferon response cGAMP interactor-1), an endoplasmic reticulum-bound DNA sensor, is highly expressed in nociceptors (Extended Data Fig. 1a), which we confirmed by *in situ* hybridization (Extended Data Fig. 1b-c). Given this pattern of expression and the variety of mediators that act through STING (Extended Data Fig. 1d), we hypothesized that STING may regulate nociception.

STING agonists suppress nociception

To determine whether STING regulates nociception, we administered synthetic (DMXAA, ADU-S100) or natural (2’3’-cGAMP, 3’3’-cGAMP) STING agonists to naïve mice via intrathecal (i.t.) injection, thereby targeting cells in the spinal cord and DRG [10]. Activation of STING induced dose-dependent antinociception in naïve mice (Extended Data Fig. 2a-c), elevating mechanical sensory thresholds for up to 48h without impairing motor coordination (Fig. 1a-d). We next tested the analgesic potential of these agonists in a chemotherapy-induced peripheral neuropathy (CIPN) model established using paclitaxel (PTX) and observed that intrathecal or systemic delivery of STING agonists could reverse mechanical and cold allodynia (Extended Data Fig. 2d-h), hallmarks of neuropathic pain [11]. STING agonists also attenuated neuropathic pain after nerve injury (Extended Data Fig. 2i-j). Given the role of STING in augmenting antitumor immunity, we tested whether STING agonists could suppress pain in a mouse model of bone cancer pain (BCP; Fig. 1e), a particularly severe and insufficiently controlled pain condition [12], and found that i.t. STING agonists could rapidly suppress cancer-induced mechanical and cold allodynia without changing local tumor burden (Fig. 1f; Extended Data Fig. 2k-l). To assess ongoing pain[13], we also performed conditioned place preference testing (CPP; Extended Data Fig. 3a). In naïve mice, i.t. morphine, but neither DMXAA nor ADU-S100 could induce place preference (Extended Data Fig. 3b-c), suggesting STING agonists do not activate the addiction and reward circuitry of the brain like morphine and other opioids [14]. To test whether DMXAA and ADU-S100 could suppress ongoing pain, we performed CPP testing in mice with CIPN or BCP and found STING agonists induced CPP in both models (Extended Data Fig. 3d-e; Fig. 1g-h). We also tested whether the opioid receptor antagonist naloxone could reverse the

antinociceptive effects of STING agonists and found that, while naloxone reversed morphine-mediated antinociception, STING agonist-mediated antinociception was not affected by naloxone (Extended Data Fig. 2m-o). Furthermore, repeated i.t. administration of DMXAA to naïve mice or mice following spared nerve injury (SNI) did not show signs of tolerance (Extended Data Fig. 2p-s). Rather, repeated administration of DMXAA attenuated SNI-induced astrogliosis (Extended Data Fig. 2t), a critical contributor to many pathological pain states [15].

STING regulates steady-state nociception

We also analyzed pain sensitivity in STING "goldenticket" mice which lack STING signaling globally (STING-gKO; STING$^{gt/gt}$). Strikingly, we observed that these mice had dramatically increased sensitivity to mechanical and cold stimuli (Fig. 1i-k). To confirm these results, we utilized a conditioned place aversion (CPA) assay in which mice were stimulated repeatedly in a preferred chamber with a very low threshold filament (0.04g) that is largely imperceptible to naïve mice [16], which resulted in CPA in STING$^{gt/gt}$ but not STING$^{+/+}$ mice (Fig. 1l-n). DRG nociceptors cultured from STING$^{gt/gt}$ mice also exhibited increased action potential firing and decreased rheobase (Extended Data Fig. 3f-j), suggesting loss of STING produces nociceptor hyperexcitability. Notably, mice lacking STING exhibited no changes in peripheral or central innervation density, total DRG neuron numbers, or sensorimotor behaviors (Extended Data Fig. 4a-n). Additionally, mice lacking STING selectively in peripheral sensory neurons (STING$^{fx/fx}$; $Na_v1.8$-Cre mice; STING-cKO)[17] revealed a similar phenotype (Fig. 1i-k), suggesting these effects are owed to sensory neuron-intrinsic STING signaling. In addition, naïve mice injected with small molecule inhibitors of STING (H-151, C176) [18] exhibited transient dose-dependent hypersensitivity (Extended Data Fig. 5a-d). STING agonists did not produce antinociception in STING$^{gt/gt}$ mice, but reduced mechanical allodynia at later timepoints in STING-cKO mice (Extended Data Fig. 5e-h), indicating that neuronal STING is required for the initial antinociceptive effects, but other cell types may contribute to the long-lasting effects. We also tested whether the antinociceptive effects of STING agonists remained intact in naïve mice in which TRPV1$^+$ nociceptors were ablated using resiniferatoxin (RTX), as these neurons exhibit the highest expression of STING (Extended Data Fig. 1a). RTX treatment led to heat insensitivity in the hot plate test and abolished the antinociceptive effects at early timepoints, while muted but statistically significant effects were retained at later timepoints (Extended Data Fig. 5i-k). To test whether adaptive immune cells important for STING agonist-mediated antitumor immunity [3] contribute to these effects, we administered STING agonists to *Prkdc*^{scid} mice, which lack mature B and T cells, and observed an unaltered time course of STING agonist-mediated antinociception (Extended Data Fig. 5l). Thus, sensory neuron-intrinsic STING signaling regulates steady-state nociception during homeostasis (Extended Data Fig. 5m), but STING signaling in multiple cell types may contribute to the prolonged antinociceptive effects of STING agonists.

STING regulates nociception via IFN-I signaling

Activation of STING drives the production of cytokines and chemokines, with IFN-I family members (IFN-α and IFN-β) chiefly among them [3]. Treatment with STING agonists led to a

robust increase of IFN-α in serum and DRG tissue, which was abolished in STING$^{gt/gt}$ mice (Fig. 2a, Extended Data Fig. 6a). We also observed high basal production of IFN-β in DRG tissue, which was reduced in STING-gKO mice (Extended Data Fig. 6b). In addition, treatment of cultured DRGs from STING-WT with ADU-S100 resulted in increased IFN-α and IFN-β in the culture medium (Extended Data Fig. 6c-d). To determine which cell types within the DRG produce IFN-I in response to STING agonists *in vivo*, we utilized *Ifnb1*$^{YFP/YFP}$ reporter mice (Extended Data Fig. 6d). Notably, we observed basal YFP as an indicator of *Ifnb1* expression in DRG neurons, and this was increased after ADU-S100 treatment (Extended Data Fig. 6e-h). Using *in situ* hybridization, we observed exceptionally high expression of the IFN-I receptor component *Ifnar1* in virtually all DRG neurons (Fig. 2b), which is confirmed by RNA-seq studies [9,19]. Similar to STING-KO/cKO mice, *Ifnar1*$^{-/-}$ (Ifnar1-gKO) mice and mice lacking *Ifnar1* selectively in sensory neurons (*Ifnar1*$^{fx/fx}$; $Na_v1.8$-Cre; *Ifnar1*-cKO) exhibited robust hypersensitivity to mechanical and cold stimuli, and CPA could be induced in *Ifnar1*-gKO with repeated stimulation using a sub-threshold filament (0.04 gram) (Extended Data Fig. 6i-m). Similarly, patch clamp recordings of DRG nociceptors revealed increased action potential firing rate and decreased rheobase in *Ifnar1*-gKO mice compared to WT littermates (Extended Data Fig. 6n-q). Nociceptors from both *Ifnar1*$^{-/-}$ and STING$^{gt/gt}$ mice exhibited increased input resistance (Extended Data Fig. 6r-s), consistent with heightened intrinsic excitability. We also confirmed peripheral and central innervation patterns, DRG neuron numbers, and other sensorimotor behaviors were normal in *Ifnar1*-gKO mice (Extended Data Fig. 7a-n). Additionally, injection of naïve mice with IFN-α or IFN-β neutralizing antibodies could recapitulate the hypersensitivity phenotype observed in *Ifnar1*$^{-/-}$ and *Ifnar1*$^{fl/fl}$;$Na_v1.8$-cre mice, and naïve mice treated with a pharmacological inhibitor of the Ifnar1 signaling adapter, Tyk2 (PF-06700841, i.t.) [20] exhibited pain hypersensitivity in a dose-dependent manner (Extended Data Fig. 8a-c). We also examined IFN-I levels and its function in DRGs (Extended Data Fig. 9a-e). Whole-mount patch clamp recordings of DRGs revealed that incubation with anti-IFN-β (300 ng/ml, 2h) increased action potential firing of DRG nociceptors (Extended Data Fig. 9d-e), providing further evidence that tonic IFN-I signaling in the DRG regulates physiological nociception.

Notably, the effects of STING agonists were completely abolished at all timepoints in *Ifnar1*$^{fl/fl}$;$Na_v1.8$-cre mice (Fig. 2c). In addition, we performed whole-mount patch clamp recordings of DRG nociceptors from PTX-treated *Ifnar1*-WT or *Ifnar1*-KO mice after *ex vivo* incubation with vehicle or ADU-S100 (Fig. 2d). Strikingly, ADU-S100 dramatically reduced action potential firing in WT mice, and this effect was abolished in *Ifnar1*-deficient neurons (Fig. 2e). Using the same incubation method in STING-WT, STING-gKO, and STING-cKO (*Sting1*$^{fl/fl}$;$Na_v1.8$-cre) mice, we confirmed that *ex vivo* incubation of DRGs with ADU-S100 led to a significant increase in IFN-α and IFN-β, which was abolished in STING-KO mice and largely abolished in STING-cKO mice (Extended Data Fig. 9a-c). To test whether i.t. administration of IFN-Is can produce antinociception, we injected naïve mice with recombinant IFN-α, IFN-β, or recombinant IFN-I (henceforth referred to as rIFN-I), an IFNAR agonist with cross-species activity. We observed that all three induced transient, dose-dependent antinociception (Extended Data Fig. 8d-f) which corresponded to the short half-life of recombinant IFN-I proteins [21]. Importantly, this effect was entirely

dependent on *Ifnar1* in peripheral sensory neurons (Fig. 2f-g). Using pharmacologic inhibitors to block distinct downstream IFN-I signaling pathways (TYK2, PI3K, and MAPK), we found that only TYK2 inhibition could abolish antinociception induced by i.t. IFN-β (Extended Data Fig. 8g-j). Given that a recent study demonstrated that high concentration of IFN-α/β (300 U) can produce mechanical hyperalgesia when administered peripherally (e.g. intraplantar, i.pl.) [22], we tested whether different routes and/or concentrations of IFN-α can differentially regulate pain. Intraplantar administration of a high dose of IFN-α (300 U) led to robust mechanical hypersensitivity for up to 3d following injection, although we observed these effects in both *Ifnar1*$^{+/+}$ and *Ifnar1*$^{-/-}$ mice (Extended Data Fig. 8k-l). Interestingly, we also found that i.t. IFN-α could block the mechanical hypersensitivity induced by intraplantar IFN-α (Extended Data Fig. 8m), suggesting that the activation of IFN-I signaling at the DRG/spinal cord levels is sufficient to produce IFN-I-mediated antinociception.

We also examined the role of STING/IFN-I signaling in cell types within the spinal dorsal horn (SDH). First, we measured the frequency and amplitude of mEPSCs from outer lamina II (IIo) spinal cord interneurons, which form a nociceptive circuit with input from C-fiber afferents and output to projection neurons [23]. Interestingly, *Ifnar1*$^{-/-}$ mice exhibited increased frequency and amplitude of mEPSCs compared to *Ifnar1*$^{+/+}$ littermates, while *Ifnar1*-cKO mice exhibited no significant differences (Extended Data. Fig 9f-h). Examination of STING expression in the SDH revealed that STING was primarily localized to Iba1^{+} microglia (Extended Data Fig. 9i-j), and STING agonists increased production of IFN-α in SDH of WT but not STING$^{gt/gt}$ (Extended Data Fig. 9k). Although IFN-β production was not increased in the presence of STING agonists, a relatively large amount of basal IFN-β was detected in WT mice, which was reduced in STING$^{gt/gt}$ mice (Extended Data Fig. 9l). Incubation of spinal cord slices with ADU-S100 decreased both the frequency and amplitude of spontaneous EPSCs (sEPSCs) from IIo interneurons (Extended Data Fig. 9m-o), suggesting STING agonists can also attenuate neurotransmission in the spinal cord in the absence of DRG cell bodies. In addition, acute perfusion with rIFN-I reduced the frequency and amplitude of mEPSCs in spinal cord slices from WT, but not *Ifnar1*-gKO mice (Extended Data Fig. 9p-r). Thus, STING-mediated IFN-I signaling in the spinal cord also plays a role in attenuating nociceptive neurotransmission.

Given our observation that STING-deficient mice exhibit lower basal levels of IFN-α/β in DRG and SDH tissue, we tested whether IFN-I ligands could rescue the hypersensitivity phenotype of STING$^{gt/gt}$ mice. Accordingly, we observed that i.t. IFN-α and IFN-β treatment of STING$^{gt/gt}$ mice could transiently rescue mechanical hypersensitivity (Extended Data Fig. 10a). Given that STING is activated by double-stranded DNA (dsDNA) through a mechanism involving the cytoplasmic DNA sensor cGAS, which generates 2’3’-cGAMP in response to dsDNA stimulation [24], we hypothesized that intracellular dsDNA may also produce antinociception through activation of the cGAS/STING pathway. Furthermore, given that IFN-I induction is a feature of both DNA sensors and RNA-sensors (such as RIG-I) [25], we also posited that intracellular RNA may produce antinociception through a STING-independent but RIG-I and IFN-I-dependent mechanism. To test these hypotheses, we activated the intracellular dsDNA or dsRNA-sensing machinery (Extended Data Fig. 10b) in naïve *Ifnar1*-WT, *Ifnar1*-cKO (*Ifnar1*$^{fl/fl}$; $Na_v1.8$-cre), STING-gKO, *cGAS*

$^{-/-}$, or *RIG-I*$^{-/-}$ (RIG-I is encoded by the *Ddx58* gene) mice via i.t. injection. The dsRNA analogue Poly(I:C) led to antinociception with similar kinetics in wild-type, STING$^{gt/gt}$ and Cgas$^{-/-}$ mice, but these effects were abolished in *Ifnar1*$^{fl/fl}$;Nav1.8-cre (*Ifnar1*-cKO) and RIG-I$^{-/-}$ mice (Extended Data Fig. 10c). By contrast, the dsDNA analogue poly(dA:dT) resulted in antinociception in wild-type and RIG-I$^{-/-}$ mice, but these effects were abolished in *Ifnar1*$^{fl/fl}$;Nav1.8-cre, STING$^{gt/gt}$ and Cgas$^{-/-}$ mice, and each of which also exhibited baseline mechanical hypersensitivity (Extended Data Fig. 10d). Thus, intracellular dsDNA and dsRNA produce IFN-I-dependent antinociception, but only dsDNA-dependent antinociception requires the cGAS–STING pathway.

To understand the mechanism underlying the antinociceptive effects of IFN-Is, we performed patch clamp recordings on DRG nociceptors. Acute perfusion with rIFN-I rapidly suppressed action potential firing, which was abolished in *Ifnar1*-deficient mice (Fig. 2h-i), and increased rheobase (Fig. 2j-k). Given that sodium channels are critical for the generation of action potentials and physiological and pathological pain [26], we posited that these effects may be due to IFN-I regulation of sodium currents. Interestingly, IFN-I perfusion led to a marked reduction in sodium currents, which was abolished in *Ifnar1*-gKO mice, which also exhibited increased baseline sodium currents (Extended Data Fig. 10e-g). To determine whether rIFN-I treatment could regulate activity of $Na_v1.7$, a sodium channel critical for physiological and pathological nociception, we recorded sodium currents from HEK-293 cells stably expressing $Na_v1.7$ following acute perfusion with rIFN-I, which led to ~20% reduction in $Na_v1.7$ currents (Extended Data Fig. 10h-i). Given that calcium currents are also critical contributors to nociception, we also recorded calcium currents. Strikingly, we observed a dramatic reduction in calcium currents following rIFN-I perfusion (~50% inhibition; Fig. 2l-m). This reduction was abolished in *Ifnar1*-gKO mice, which exhibited no change in basal calcium currents (Fig. 2m-n). Thus, IFN-I signaling can directly suppress nociceptor excitability via multifaceted suppression of sodium and calcium channel activity.

STING agonists produce analgesia in NHPs

To challenge the translational relevance of our findings, we tested whether STING activation can suppress nociception in non-human primates (NHPs), rhesus macaques (*Macaca mulatta*) using a menthol gel-induced cold allodynia assay (Fig. 3a). As expected, ADU-S100 administration through a spinal catheter produced long-lasting and dose-dependent analgesia (Fig. 3b), which was accompanied by a substantial increase in cerebrospinal fluid (CSF) levels of IFN-β (Fig. 3c). These effects were observed at doses much lower than those used in murine models (3 nmol vs. 35 nmol), indicating ADU-S100 may possess better selectivity for primate/human STING. We next recorded action potentials from dissociated NHP DRG nociceptors and found that acute rIFN-I perfusion robustly suppressed action potential firing and increased rheobase (Fig. 3d-f). Finally, we tested whether rIFN-I treatment could alter the excitability of human DRG neurons (hDRGs). Although we were unable to record action potentials in hDRGs, rIFN-I perfusion consistently hyperpolarized small-diameter hDRG neurons (Fig. 3g-i). Collectively, these data reveal that STING pathway activation induces long-lasting analgesia in NHPs, and IFN-I ligands directly suppress excitability of mouse, NHP, and human nociceptors through modulation of sodium and calcium channel function (Fig. 3j).

Discussion

Our study identifies the STING/IFN-I signaling axis as a master regulator of nociception which regulates steady-state pain sensitivity as well as chronic pain in several pathological conditions. From an evolutionary perspective, the use of the STING/IFN-I signaling pathway to inhibit pain while concurrently activating the immune response following a challenge is noteworthy, as the stimuli leading to the activation of the IFN-I pathway (e.g. radiation, cancer, infection) tend to be quite painful [7,8]. Thus, activation of the IFN-I pathway in sensory neurons may be a hardwired mechanism to suppress pain in challenging conditions. Our data indicate that STING-mediated IFN-I signaling acts through an autocrine and/or paracrine mechanism in peripheral sensory neurons, which acts via a noncanonical mechanism in which IFN-I/IFNAR signaling leads to exceptionally rapid suppression of sodium channel and calcium channel function (Fig. 3j). Importantly, the intrathecal doses of STING agonists required to produce analgesia in NHPs are quite low compared to that of morphine (3 vs. 100 nmol) [27], with effects persisting for much longer [28]. Thus, STING agonists, at low concentrations, appear to offer significant advantages to even the most aggressive pain pharmacotherapies without showing signs of tolerance with repeated injections. Despite these promising results, it is important to consider which chronic pain conditions are severe enough to warrant immunomodulation, which could also yield unwanted side effects [29]. The majority of patients with advanced-stage cancers experience severe pain, but fewer than half of these patients report effective pain relief [30]. Our observation that STING agonists provide substantial antinociception in an exceptionally painful model of bone cancer pain warrant immediate further exploration. This is compounded by the clinical promise that STING agonists have shown as cancer immunotherapy adjuvants, promoting immune cell-mediated antitumor immunity [3,31,32]. Taken further, we propose that these STING-dependent functions (e.g. antitumor immunity and antinociception) could act synergistically through distinct actions on immune cells and peripheral nociceptors.

METHODS

No statistical methods were used to predetermine sample size. Animals were randomly assigned to treatment groups. The investigators were double-blinded to experimental treatments during experiments and outcome assessment.

Reagents

This study utilized the following reagents and concentrations: DMXAA (various concentrations, as indicated; Cayman Chemical, 14617), ADU-S100 (various concentrations, as indicated; Chemietek, CT-ADUS100), 2’3’-cGAMP (10 μg, i.t.; Invivogen, tlrl-nacga23-02), 3’3’-cGAMP (10 μg, i.t.; Invivogen, tlr-nacga), poly(dA:dT)/LyoVec (1 μg, i.t.; Invivogen, tlrl-patc), poly(I:C)/LyoVec (1 μg, i.t.; high molecular weight; Invivogen, tlrl-piclv), clonidine hydrochloride (35 nmol, i.t.; Millipore Sigma, C7897), naloxone hydrochloride dihydrate (10 mg/kg, i.p.; Millipore Sigma, N7758), morphine sulfate (2 nmol, i.t.; WEST-WARD Pharmaceuticals), recombinant mouse IFN-α A (various concentrations, as indicated; PBL Assay Science, 12100-1), recombinant mouse IFN-β

(various concentrations, as indicated; PBL Assay Science, 12410-1), recombinant universal type-I interferon (various concentrations, as indicated; PBL Assay Science, 11200-1), H-151 (10 nmol, i.t.; Cayman Chemical, #25857), C-176 (10 nmol, i.t.; Cayman Chemical, #25859), PF-06700841 tosylate salt (various concentrations, as indicated; Millipore Sigma, PZ0345-5MG), U0126 (1 μg, i.t.; Millipore Sigma, 19-147), LY294002 (1 μg; Millipore Sigma, L9908), anti-mouse IFN-α neutralizing antibody (300 ng/mouse, i.t.; PBL Assay Science, 32100-1), anti-mouse IFN-β neutralizing antibody (300 ng/mouse, i.t.; PBL Assay Science, 32400-1), rabbit polyclonal IgG control (300 ng/mouse, i.t.; Biolegend, CTL-4112), paclitaxel (Millipore Sigma, T7191), and resiniferatoxin (Millipore Sigma, R8756).

Genetic mouse models

All mouse procedures were approved by the Duke University Institutional Animal Care and Use Committee (IACUC) and complied with relevant ethical guidelines. Mice were housed in an animal facility approved by the Association for Assessment and Accreditation of Laboratory Animal Care (AAALAC) under a 12h light/dark cycle with food and water available *ad libitum*. All commercially-available genetic mouse models were obtained from Jackson Labs and maintained on a C57BL/6J background, including: *Ifnb1*^{YFP} reporter mice (strain #010818)[33], STING "goldenticket" knockout mice[34] (STING$^{gt/gt}$; strain #017537), STING floxed/conditional knockout mice[35] (STING$^{fx/fx}$; strain #031670), *Ifnar1* global knockout mice (*Ifnar1*$^{-/-}$; strain #028288), *Ifnar1* floxed/conditional knockout mice[36] (*Ifnar1*$^{fx/fx}$; strain #028256), cGAS knockout mice[37] (*cGAS*$^{-/-}$; strain #026554), and RIG-I knockout mice (*RIG-I*$^{-/-}$; strain # 46070-JAX). Nav1.8-Cre mice[38], also maintained on a C57BL/6J background, were a gift from Rohini Kuner (University of Heidelberg). NOD.CB17-Prkdc^{scid} mice were also obtained from Jackson Labs (strain #001303) and maintained in a NOD/ShiLtSz genetic background. Unless otherwise noted, all experiments were conducted in adult (8-12-week-old) mice. Animals were randomly assigned to each experimental group. Both males and females were included in each group in a sex-matched manner. The data from both sexes were combined and used relatively equally throughout this study, as no sex differences were observed. The complete sample sizes and sex are summarized in Supplementary Table 1.

Mouse pain models

The chemotherapy-induced peripheral neuropathy (CIPN) model of chronic neuropathic pain was established as we have done previously[39], using 8-10-week-old CD-1 (strain #022, Charles River) mice injected with paclitaxel (2 mg/kg i.p.) every other day, with 4 injections total. The chronic constriction injury (CCI) model of neuropathic pain was also produced using 8-10-week-old CD-1 under isoflurane anesthesia[40]. Briefly, the right sciatic nerve was exposed above the hip and two ligatures (7-0 Prolene) were placed around the nerve 1 mm apart located proximal to the trifurcation. Ligatures were loosely tied until a subtle flick of the ipsilateral hind limb was observed. CD-1 mice were also used to establish the SNI model, which was generated by tightly ligating the tibial and common peroneal nerves followed by transection and removal of a −3 mm portion of the nerve. The sural nerve was left intact and contact or stretching of this nerve was avoided[41]. To establish the syngeneic bone cancer pain (BCP) model, 8-10-week-old C57BL/6J mice (strain #000664, Jackson Labs) were utilized, as the Lewis lung carcinoma cell line LLC1 (LL/2; ATCC CRL-1642)

was originally generated in C57BL/6J mice. Mice were anesthetized with isoflurane and the left leg was shaved, disinfected with 10% povidone-iodine, and a 1 cm superficial incision was made to expose the patellar ligament. A 25-gauge needle was inserted at the intercondylar notch of the left femur into the femoral cavity, followed by needle replacement with a 10 μl Hamilton syringe microinjector containing a 2 μl suspension of LLC cells (2 x 10^5 cells) followed by a 2 μl gelatin sponge solution to enable closure of the injection site[12]. All mice were housed and monitored in accordance with AAALAC standards and Duke IACUC guidelines that pertained to each model.

Reflexive-based sensory testing in mice

All behavioral testing in mice was performed in a specialized humidity- and light-controlled mouse behavior facility maintained at 21-24°C, with testing conducted between the hours of 8:00-16:00. Mice were habituated to the testing environment for at least 2 days prior to baseline testing. All tests were performed by an experimenter who was blinded to experimental conditions, including genotypes and drug treatment. For multi-day experiments using STING agonists, mice were tested in the same room at approximately the same time each day. To measure mechanical sensitivity, mice were confined to individual chambers with non-transparent borders on an elevated mesh rack, preventing mice from visualizing or interacting with one another during the testing period. Mouse hindpaws were stimulated with a series of von Frey filaments with logarithmically increasing stiffness (0.02-2.56g, Stoelting), which was applied perpendicularly to the central plantar surface. We determined the 50% paw withdrawal threshold using the up-down method[42]. We also assayed mechanical allodynia by determining paw withdrawal frequency to repeated stimulation (10 times, with ~1-2 minutes between each stimulation) using a subthreshold 0.16g von Frey filament, which ordinarily does not elicit reflexive withdrawal. To test cold sensitivity, mice were again placed on an elevated metal mesh floor in isolated chambers, and a ~20 μl acetone drop was applied to the central plantar surface of the mouse hindpaw using a pipette. The duration of time that animals exhibited nociceptive behaviors (paw lifting, licking, flicking) was recorded using a stopwatch immediately following acetone application.

Naloxone reversal and repeated STING agonist administration

To test whether the opioid receptor antagonist naloxone could reverse morphine or STING agonist-induced antinociception, naloxone was administered (10 mg/kg, i.p.) at the following timepoints after drug delivery: morphine (2 nmol, i.t., 30 minutes), DMXAA (35 nmol, i.t., 4h after administration), ADU-S100 (35 nmol, i.t., 4h after administration). Following naloxone delivery, mice were tested within 15 minutes. For the experiments testing whether mice developed tolerance to the effects of STING agonists, vehicle or DMXAA (35 nmol) were administered via i.t. injection. Naïve mice received five single injections at D0, D3, D6, D9, and D12, with testing each day 4h after injection. SNI mice received injections on two consecutive days beginning on D7 (D7 and D8) and every 48h afterwards following the conclusion of sensory testing (D10, D12, D14, D16, and D18). Spinal cords (L4-L5) were collected for analysis of glial cell activation at D21 following SNI.

Motor, locomotor, and sensorimotor behaviors

Rotarod testing was performed to assess motor coordination, as we have done previously[43]. Prior to testing, mice were placed in the behavioral room for 30 minutes. We used an accelerating protocol (4-45 RPM over 300 seconds). Each mouse was tested in 3 daily sessions, each of which consisted of 3 independent trials which were separated by at least 10-minute intervals. The data displayed represent the average fall latency on the 3rd day of testing. To test overall locomotor activity, we performed open field testing in which mice were placed in the center of a 45 x 45 cm chamber and locomotor activity was recorded by an overhead webcam connected to a laptop computer, and animals' movements were tracked for 30 minutes using ANY-Maze. The data displayed represent the total locomotor activity during the 30-minute period. We also tested sensorimotor behaviors using the plantar tape test (also known as the adhesive removal test)[44]. Briefly, several days prior to the experiment, mice were acclimated to handling (scruffing). On the day of the experiment, mice were acclimated to a standard mouse cage without bedding for 60s. Mice were then gently immobilized, and a 3x4 mm tape was firmly applied to the plantar surface of the left hindpaw such that it covered the glabrous skin. The mice were returned to the testing cage, and the latency (in seconds) to remove the tape was recorded by an experimenter blinded to the genotypes of the animals.

Conditioned place preference (CPP) assay

To test whether STING agonists would induce CPP in naïve mice, we used a three repeated-pairing conditioning protocol, as a single trial was found to be insufficient to induce place preference in the morphine control group. To test whether STING agonists could induce CPP in chronic pain (CIPN and BCP) models, a measure of ongoing or spontaneous pain, we used a single-trial pairing protocol, as this was sufficient to induce robust CPP in the clonidine control group. These observations are consistent with previous reports[45,46]. All mice underwent 3 days of preconditioning habituation in a temperature- and humidity-controlled room under low-light conditions between 08:00-16:00 in a two compartment CPP chamber (Med Associates Inc.). The two compartments differed by both visual and tactile cues. On the 4th day, animal behavior was video-recorded using a webcam connected to a laptop computer, and animal movement was automatically tracked for 15 minutes using the ANY-Maze software (Stoelting). Baseline recordings revealed that mice generally formed a slight preference to one chamber. Mice exhibiting strong preference (>80% of time spent in one chamber) were not used for the experiments. On the conditioning day(s) (day 5 for single trial; day 5-7 for repeated trials), two pairing sessions were performed, with vehicle pairing in the AM session and drug treatment (e.g. vehicle or drug) in the PM session, separated by 4h. In the AM session, mice always received vehicle (10 μl saline, delivered via i.t. injection under isoflurane anesthesia) and were immediately placed in their preferred CPP chamber for 2h. In the PM session, mice received drug treatment (10 μl, delivered via i.t. injection under brief isoflurane anesthesia) and were placed in their non-preferred chamber immediately (PBS, morphine, and clonidine) or 4h later (DMXAA, ADU-S100), time points corresponding to the peak antinociceptive effects of these agents. 24h after the completion of the pairing experiments, mice were placed in the CPP test box with access to both chambers and behavior was recorded for 15 minutes and analyzed using the ANY-Maze software for chamber preference. CPP score was calculated as the inverse of the time spent

in the preferred chamber according to: [post-preference (sec) – pre-preference (sec)]. Vehicle served as a negative control for these experiments, while morphine (three trials/naïve mice) or clonidine (single trial/ongoing pain) served as positive controls.

Conditioned place aversion (CPA) assay

A modified CPA assay was used based on a previous report [16]. Briefly, male and female mice lacking *Ifnar1* or STING (and their wildtype littermates) were habituated for three days (30 minutes each) to a small custom-designed two-chamber CPA apparatus which was placed on an elevated mesh rack. Each chamber contained unique visual cues (black and white cross-hatching or plain white walls) and measured approximately 4.5 x 9 inches across. On the final day of habituation, baseline (BL) preferences were video-recorded for 10 minutes and movement was tracked using the ANY-Maze software. Following BL measurements, animals were sequestered to their preferred chamber and pairing was conducted by repeatedly stimulating the left hindpaw once every 10 seconds for 10 minutes using a 0.04g filament, which is normally innocuous and does not elicit withdrawal responses or CPA in naïve mice. No mice exhibited greater than 65% preference for either chamber, and thus, all mice in which BLs were recorded were used in the experiment. After pairing, mice were returned to their home cage for 20 minutes, after which time they were returned to the CPA chamber with equal access to both chambers. Post-pairing behaviors were video recorded for 10 minutes and movement was again tracked using ANY-Maze software. CPA score was calculated as the time spent in the paired chamber according to: [post-preference (sec) – pre-preference (sec)].

Behavioral testing in non-human primates

Five adult rhesus monkeys (*Mucaca mulatta*, 9.3-13.8 kg) were maintained in an AAALAC-approved facility at Wake Forest University School of Medicine in accordance with Wake Forest University IACUC regulations. Animals were individually housed in temperature- and humidity-controlled species-specific rooms maintained in a 12h light/12h dark cycle. All animals have been previously trained in the tail-withdrawal assay. All experimental procedures were conducted in accordance with the *Guide for the Care and Use of Laboratory Animals* standards adopted by the NIH. Drug infusion was through a previously implanted spinal catheter. Behavioral testing was performed by an experimenter who was blinded to the drug being administered. A cold-water tail-withdrawal assay was used to evaluate nociceptive responses to 16°C water with a cut-off of 20 sec. 0.3 mL of 2% menthol gel (Millipore Sigma) was applied to the tail for 3 minutes to induce transient and reversible cold allodynia. The antinociceptive effects of ADU-S100 were measured at different time points i.e., before and 5h, 24h, and 29h after intrathecal administration.

Culture of LLC cells and measurement of local tumor burden

Murine LLC cells were cultured in high glucose (4.5 g/L) Dulbecco's Modified Eagle Medium (DMEM; ThermoFisher) supplemented with 10% fetal bovine serum (Gibco, ThermoFisher) and 1% Antibiotic-Antimycotic solution containing penicillin, streptomycin, and Amphotericin B (ThermoFisher, 15240062). No testing was performed for mycoplasma contamination. Cells were cultured in the presence of 5% CO_2 at 37°C. Cells were passaged using a 0.05% trypsin digest once they achieved 70% confluency. Prior to *in vivo* injection,

cells were harvested with 0.05% trypsin digestion followed by several washes in PBS. Cell counts were performed using a hemocytometer and diluted to achieve a suspension of $1x10^8$ ml^{-1} cells in PBS. To determine whether i.t. STING agonists altered local tumor burden induced by femoral inoculation with LLC cells, mice were lightly anesthetized with isoflurane at the conclusion of the experiment, followed by measurement of the total circumference of the widest aspect of the thigh, which accurately reflects tumor burden [48]. Ratios were computed between the ipsilateral (LLC-inoculated) and contralateral (tumor-free) legs.

Drug delivery

All drugs were dissolved in sterile saline or PBS, which was used as the corresponding vehicle control, with the exception of DMXAA, which was first dissolved in PBS containing 0.75% $NAHCO_3$ and was further diluted 10-fold prior to experimentation, and H-151 and C-176, which were diluted in PBS containing 5% DMSO and 0.0625% Tween-20 due to poor solubility[18]. For the experiments utilizing i.t. 2'3'-cGAMP and 3'3'-cGAMP complexed with Lipofectamine 2000 (ThermoFisher, 11668), 10 μg 2'3'-cGAMP or 3'3'-cGAMP was incubated at room temperature for 30 minutes in sterile PBS with 3 μl Lipofectamine 2000. In this case, the vehicle control was 3 μl Lipofectamine 2000 in PBS, as in a previous study which used this approach[50] . Drug concentrations and route of administration are generally provided in the figures or figure legends. DMXAA and ADU-S100 were generally used at a concentration of 35 nmol (i.t.), administered via two injections 24h apart. For experiments utilizing rabbit anti-IFN-α or -β neutralizing antibodies, a polyclonal rabbit IgG antibody served as the control. Antibodies were utilized *in vivo* at 300 ng/mouse or *in vitro* at 300 ng/ml. Paclitaxel was administered via repeated i.p. injections every other day for 4 days at a dose of 2 mg/kg. For the whole mount DRG recordings, young mice (4-6 weeks) were administered a single 6 mg/kg dose one week prior to the experiment. All intrathecal injections were performed under brief anesthesia with 2-2.5% isoflurane. Drugs administered by intrathecal injection were preceded by shaving a small area on the back corresponding to the injection site, followed by spinal puncture using a 30-gauge needle between the L5-L6 levels to deliver a maximum of 5-10 μl into the cerebrospinal fluid. Successful intrathecal injection was always confirmed by a brisk tail-flick upon delivery. For the experiments involving intraplantar (i.pl.) injection, IFN-α was dissolved in sterile saline and administered at the concentrations indicated in the figures in a total volume of 20 μl, administered under 2-2.5% isoflurane anesthesia to minimize animal stress. For these experiments, vehicle (saline) or IFN-α were slowly and carefully expressed into the left dorsal hindpaw of anesthetized mice and allowed to perfuse the tissue for ~20 seconds prior to removal of the needle. Mice were monitored for ~30 seconds after removal of the needle to ensure that the solution did not express from the tissue. Mechanical sensory testing was done anteriorly and care was taken to avoid Von Frey filament stimulation of the injection site.

ELISA

Mouse high-sensitivity IFN-α ELISA kit (42115-1) and IFN-β ELISA kit (42410-1) were purchased from PBL Assay Science and performed on serum, DRG lysate, or cell culture medium according to the manufacturer's instructions. Serum was obtained from whole blood

through cardiac puncture at the time of euthanasia, followed by incubation for 30 minutes at 35°C to promote clotting. Subsequently, samples were centrifugated at 4°C at 2,500xg for 15 minutes, followed by careful isolation of serum (supernatant). For ELISA on cell culture medium, samples were first concentrated approximately 10-fold using Amicon centrifugal filters (Millipore Sigma, UFC8030). DRGs were lysed by mechanical homogenization in a pH 7.4 CHAPS lysis buffer (FivePhoton Biochemicals, CIB-1-7.4-60) supplemented with a protease inhibitor cocktail (Millipore Sigma, 11697498001) and phosphatase inhibitor cocktail (FivePhoton Biochemicals, PIC1). For DRG lysate, Pierce BCA (ThermoFisher, 23225) assays were performed according to the manufacturer's instructions to quantify protein concentration, and ELISA results are reported normalized to protein concentration (pg/mg DRG tissue). To measure IFN-β levels in cerebrospinal fluid (CSF) isolated by spinal catheter from NHPs, we utilized a cynomolgus IFN-β ELISA kit (PBL Assay Science, 46415-1), which was performed using 50 μl CSF according to the manufacturer's instructions. Standard curves were performed in all experiments and values interpolated using GraphPad Prism version 8.

In situ hybridization (ISH)

Mice were deeply anesthetized with isoflurane and transcardially perfused with 25 ml PBS followed by 25 ml 4% paraformaldehyde/1% picric acid. Following perfusion, L3-L5zen spinal cords or DRGs were isolated and post-fixed overnight at 4°C in the same fixative. Tissues were subsequently washed several times in PBS, followed by cryopreservation using a sucrose gradient. tissues were then embedded in OCT medium (Tissue-Tek) and cryosectioned to produce 14 μm-thick sections, which were mounted onto charged slides. Each tissue block (and thus, each slide) contained both WT and KO tissues to account for any variability in staining between slides, and to control for the specificity of RNAscope probes targeting STING (*Tmem173*) or *Ifnar1*. *In situ* hybridization was performed using the RNAscope system (Advanced Cell Diagnostics) in accordance with the manufacturer's instructions, using a protocol tailored to the Multiplex Fluorescent Kit v2. We used probes directed against murine *Ifnar1* (catalog 512971, NM_010508.2) and murine STING (*Tmem173*; catalog 413321, NM_028261.1). Following the completion of the RNAscope protocol, immunohistochemistry was performed as described in the next section. The *in situ* hybridization experiments were repeated in three independent experiments.

Immunohistochemistry and imaging

Adult mice were deeply anesthetized with isoflurane and perfused through the ascending aorta with 20-25 ml PBS, followed by 4% paraformaldehyde/1% picric acid. Following perfusion, L3-L5 DRGs, L3-L5 spinal cord segments, or mouse plantar hindpaw skin were removed and post-fixed in the same fixative overnight. Tissues were cryopreserved and sectioned in the same manner described for ISH. Sections were blocked for 1h at room temperature in a solution containing 1% BSA, 0.1% triton X-100, 5% normal donkey serum, and mouse-on-mouse blocking reagent (if mouse antibodies were used) in accordance with the manufacturer's instructions. Sections were stained in a humidified chamber overnight at 4°C with the following primary antibodies: anti-GFAP (mouse, 1:2000, Millipore Sigma, MAB360), Iba1 (rabbit, 1:500, Wako, 019-19741), anti-β Tubulin III (mouse, TuJ1; 1:1000, Millipore Sigma, T8578), anti-CGRP (guinea pig, 1:1000, Peninsula, T-5027), and anti-GFP

(chicken, 1:2000, Abcam, ab13970). The next day, sections were washed several times, followed by incubation with Isolectin GS-IB_4-488 conjugate (1:500, ThermoFisher, I21411), Nissl/NeuroTracer-640 (1:200, ThermoFisher, N21483), or species-specific secondary antibodies conjugated to −488, −555, or −633 fluorophores purchased from Biotium, which were raised in donkey (1:400), stained in a humidified chamber overnight at 4°C. Sections were subsequently washed and coverslipped using a few drops of DAPI Fluoromount-G mounting medium (Southern Biotech, 0100-20). Stained sections were examined using a Nikon fluorescent microscope, and images were captured with a mounted CCD Spot camera. For high resolution imaging, images were also captured using a Zeiss LCM 880 confocal microscope with a z-step size of 1 μm, with 10-12 steps. For images captured on the confocal microscope, maximum projections were produced using the Zeiss ZEN software package (v3.2). Images directly comparing two groups (e.g. WT and KO mice) were taken using the same acquisition settings.

Quantification of total cell numbers and innervation density

Quantification of total neuron numbers was performed by counting TuJ1+ neurons with DAPI+ nucleoli in the L5 DRG, counting every third section. To quantify immunostaining in the superficial dorsal horn (IB4/CGRP density for innervation staining; GFAP, Iba1, and DAPI for quantification of glial cell activation), the Image J plugin Fiji was utilized to draw a box narrowly around the relevant regions followed by quantification of pixel density by an experimenter blinded to the treatment groups. For the quantification of CGRP and IB4 in the SDH, the data reported (normalized density) represent the pixel intensity of each signal normalized to the area, reported as arbitrary units (A.U.). For the quantification of glial cell reaction, values represent the ratio of pixel density for each channel on the ipsilateral (SNI-injured) side normalized to the contralateral (uninjured) side. To quantify the density of nerve fibers in the glabrous skin of the hindpaw, we counted the number of $TuJ1^+$, $CGRP^+$, or $IB4^+$ nerve fibers (>5μm in length), in 3-5 separate sections for each animal. Data display the average number of nerve fibers positive for each marker per mm^3. In all cases, the images were quantified by an experimenter blinded to animal genotypes.

Whole-cell patch clamp recordings in dissociated mouse DRG neurons

DRGs were removed under sterile conditions from 4-6-week-old male and female mice and digested with a collagenase (1.25 mg/ml; Roche)/dispase-II (2.4 U/ml; Roche) solution for 90 minutes at 37°C, followed by incubation in 0.25% trypsin for 10 minutes at 37°C. Cells were mechanically dissociated with a flame-polished Pasteur pipette and plated in a 50 μl bead for 30 minutes prior to flooding the chamber. Cells were plated on glass cover slips coated with 0.5 mg/ml poly-D-lysine (Millipore Sigma, A-003-E) and cultured in a Neurobasal medium (Gibco, ThermoFisher) supplemented with 10% FBS, 2% B27 supplement (Gibco, ThermoFisher), and 1% penicillin-streptomycin (Gibco, ThermoFisher) at 37°C in 5% CO_2 for 24h prior to recordings. Coverslips were transferred to a 300 μl recording chamber continuously perfused (~3 ml/min) with artificial cerebrospinal fluid (ACSF) where small-diameter DRG neurons (<25 μm) could be identified using a 40x water-immersion objective on an Olympus BX51WI microscope. Whole-cell patch-clamp configuration was made, and current clamp mode was performed to record action potentials. The action potentials were evoked by current injection steps from 0 – 130 pA with an

increment of 10 pA in 600 ms. Rheobase was measured by injecting currents from 0 pA with an increment of 10 pA in 30 ms. Patch pipettes were pulled from borosilicate capillaries (Chase Scientific Glass Inc.) and filled with a pipette solution containing (in mM): 126 potassium gluconate, 10 NaCl, 1 $MgCl_2$, 10 EGTA, 2 Na-ATP, and 0.1 Mg-GTP, adjusted to pH 7.3 with KOH. The external solution was composed of (in mM): 140 NaCl, 5 KCl, 2 $CaCl_2$, 1 $MgCl_2$, 10 HEPES, 10 glucose, adjusted to pH 7.4 with NaOH. The resistance of pipettes was 4-5 MΩ. Series resistance was compensated for (>80%) and leak subtraction was performed. Data were low-pass filtered at 2 KHz and sampled at 10 KHz. Data were recorded and analyzed using the pClamp10 (Axon Instruments) software. Recordings from DRG neurons (<25 μm) were performed between 24-48h of plating. The vehicle or IFN-I was perfused for 3 min, and APs and rheobase were recorded before (control) and 4-5 min after the onset of the perfusion of the vehicle or IFN-I.

Primary culture and whole cell patch clamp recordings from NHP DRG neurons

Lumbar DRGs were isolated from disease-free NHPs and delivered on ice within 4h of death. Neurons were dissociated, plated, and cultured as described for mouse DRG neurons. 24h after plating, whole-cell patch clamp recordings were performed on small-diameter DRG neurons (<50 μm) at room temperature using patch pipettes with a resistance of 2-3 MΩ. Whole-cell patch-clamp configuration was made, and current clamp mode was performed to record action potentials. The action potentials were evoked by current injection steps from 0 – 580 pA with an increment of 20 pA in 1500 ms. Rheobase was measured by injecting currents from 0 pA with an increment of 15 pA in 60 ms. The experimental setup and data recording were performed as in the section detailing patch clamp recordings on mouse DRG neurons. The vehicle or IFN-I was perfused for 3 min, and APs and rheobase were recorded before (control) and 4-5 min after the onset of the perfusion of the vehicle or IFN-I.

Primary culture and whole cell patch clamp recordings from human DRG neurons

Non-diseased human DRGs (hDRGs) were obtained from three donors through NDRI (Philadelphia, PA) with permission of exemption from Duke IRB. Postmortem lumbar hDRGs were delivered in ice-cold culture medium within 48–72 hours of death. Upon delivery, hDRGs were rapidly dissected from nerve roots and minced in a calcium-free HBSS. hDRGs were digested at 37°C in a humidified 5% CO_2 incubator for 120 min with a collagenase (1.25 mg/ml; Roche)/dispase-II (2.4 U/ml; Roche) solution in HBSS. hDRGs were mechanically dissociated using fire-polished pipettes, passed through a 100 μM nylon mesh filter, and centrifuged (500xg for 5 min). Cells were resuspended, plated on 0.5 mg/ml poly-D-lysine-coated glass coverslips, and grown in culture medium identical to mouse and NHP DRGs. Patch clamp recordings were conducted in small-diameter (<55 μm) hDRG neurons[51]. While the condition of hDRG neurons generally did not permit consistent recording of evoked action potentials, we recorded changes in membrane potential following perfusion with vehicle or IFN-I (30 U/ml), conducted as in the section detailing patch clamp recordings on mouse DRG neurons.

Whole-cell patch clamp recordings in whole-mount DRGs *ex vivo*

To test the effects of anti-IFNβ neutralizing antibodies, naïve male and female mice were utilized. For the experiment testing the effects of ADU-S100 in *Ifnar1*$^{+/+}$ or *Ifnar1*$^{-/-}$ mice following PTX treatment, male and female mice of the indicated genotypes were treated with a single dose of 6 mg/kg PTX followed by recording 1 week later. To perform whole-cell patch clamp recordings in whole-mount DRGs, L1-L5 DRGs were carefully isolated and placed in oxygenated ACSF. Using a stereoscope, peripheral and central DRG projections and connective tissue were dissected away. DRGs were lightly digested for 20 minutes using an enzymatic mixture consisting of 0.32 ml collagenase A (1 mg/mL) and Trypsin (0.25%). Intact DRGs were then incubated in ACSF oxygenated with 95% O_2 and 5% CO_2, supplemented with the relevant treatment: (1) 300 ng/ml rabbit polyclonal IgG control or rabbit anti-IFNβ for 2-3 hours at 37°C; or (2) vehicle (PBS) or 30 μM ADU-S100 in PBS for 2-3 hours at 37°C. Following incubation, DRGs were transferred to a recording chamber, where neurons could be visualized using a 40x water-immersion objective on an Olympus BX51WI microscope. The recording chamber was continuously perfused (2-3 ml/min) with ACSF. The pipette solution contained 140 mM KCl, 2 mM $MgCl_2$, 10 mM HEPES, 2 mM Mg-ATP at pH 7.4. The resistance of the glass pipettes was 8-10 MΩ. Data were acquired and analyzed using the pClamp10 (Axon Instruments) software.

Whole cell patch clamp recording of sodium and calcium currents *in vitro*

For sodium current recordings, HEK-hNav1.7 stable cell line was purchased from SB Drug Discovery (Glasgow, United Kingdom). Cells were cultured in MEM containing 10% FBS, 1% streptomycin/penicillin, L-glutamine (2 mM) and blasticidin (0.6 mg/ml). Whole-cell patch-clamp recordings on HEK293 cells and DRG neurons were conducted at room temperature according to the protocol for whole cell patch clamp in dissociated DRG neurons. In voltage-clamp experiments, transient Na^+ currents were evoked by a test pulse to 0 mV from the holding potential (−70 mV). Calcium current was evoked in DRG neurons by applying a 40-ms step depolarization to −10 mV from −80 mV[52]. For calcium recordings, the external solution contained the following: 135 mM TEA-Cl, 1 mM $CaCl_2$, 10 mM HEPES, 4 mM $MgCl_2$ and 0.1 μM tetrodotoxin (TTX), adjusted to a pH of 7.4 with TEA-OH. The pipette solution contained 126 mM CsCl, 5 mM Mg-ATP, 10 mM EGTA and 10 mM HEPES, adjusted to a pH of 7.3 with CsOH.

Whole-cell patch-clamp recording in mouse spinal cord slices

4 to 6-week-old mice were anesthetized with urethane (1.5-2.0 g/kg, i.p.). The lumbosacral spinal cord was quickly removed and placed in ice-cold dissection solution (240 mM sucrose, 25 mM $NaHCO_3$, 2.5 mM KCl, 1.25 mM NaH_2PO_4, 0.5 mM $CaCl_2$, and 3.5 mM $MgCl_2$), equilibrated for at least 30 minutes with 95% O2 and 5% CO2. After extraction of the spinal cord under anesthesia, animals were rapidly euthanized via decapitation. Transverse spinal slices (300 to 400 μm) were prepared using a vibrating microtome (VT1200S Leica). The slices were incubated at 32°C for at least 30 min in ACSF equilibrated with 95% O2 and 5% CO2. The slices were placed in a recording chamber and completely submerged and perfused at a flow rate of 2 to 4 ml/min with ACSF saturated with 95% O2 and 5% CO2 at room temperature. Lamina II neurons in lumbar segments

were identified as a translucent band under a microscope (BX51WIF; Olympus) with light transmitted from below. Whole-cell voltage-clamp recordings were made from outer lamina II neurons using patch pipettes[53]. The patch pipette solution used to record sEPSCs contained 135 mM K-gluconate, 5 mM KCl, 0.5 mM $CaCl_2$, 2 mM $MgCl_2$, 5 mM EGTA, 5 mM HEPES, and 5 mM Mg–ATP (pH 7.3 adjusted with KOH). The patch pipettes had a resistance of 8 to 10 M. The sEPSC recordings were made at a holding potential (*V*H) of −70 mV in the presence of 10 μM picrotoxin and 2 μM strychnine. mEPSCs were recorded in the presence of 0.5 μM TTX, perfused 4 min prior to drug application. Signals were acquired using an Axopatch 700B amplifier. The data were stored and analyzed with a PC using pCLAMP 10.3 software.

Data collection, statistics, and transparency

All data are expressed as the mean ± s.e.m., as indicated in the figure legends. In most cases, each data point corresponds to an individual animal. For electrophysiology data, each data point corresponds to an individual neuron, with neurons from at least 3 separate animals/subjects analyzed in all cases, specified in Supplementary Table 1. The sample sizes utilized in each experiment were based on our previous studies [12,40,52]. All data were included in the analyses (no outliers removed). In some cases, indicated within the figure legends, sample sizes are larger than would be necessary to observe differences between groups because experiments were repeated multiple times to ensure reproducibility with all relevant controls. All experimental data shown has been reliably reproduced by multiple lab members. All statistical analyses were completed using GraphPad Prism 8. Unless otherwise noted in figure legends, behavioral and biochemical data and some electrophysiological data were analyzed using two-way ANOVA with Dunnett's *post-hoc* test to account for multiple comparisons. For the CPP assay, each experimental group was compared with the vehicle treatment group using one-way ANOVA with Fisher's least significant difference *post-hoc* test. A two-tailed t-test was utilized to compare two groups when analyzing sensory neuron numbers and innervation densities. Electrophysiological data were tested using two-tailed t-test (for two groups) or two-way ANOVA (for multiple time points) with Dunnett's *post hoc* test. The criterion for statistical significance was defined as $p < 0.05$. Throughout this manuscript, asterisks correspond to the following significance levels: * $p < 0.05$, ** $p < 0.01$, *** $p < 0.001$, **** $p < 0.0001$.

Extended Data

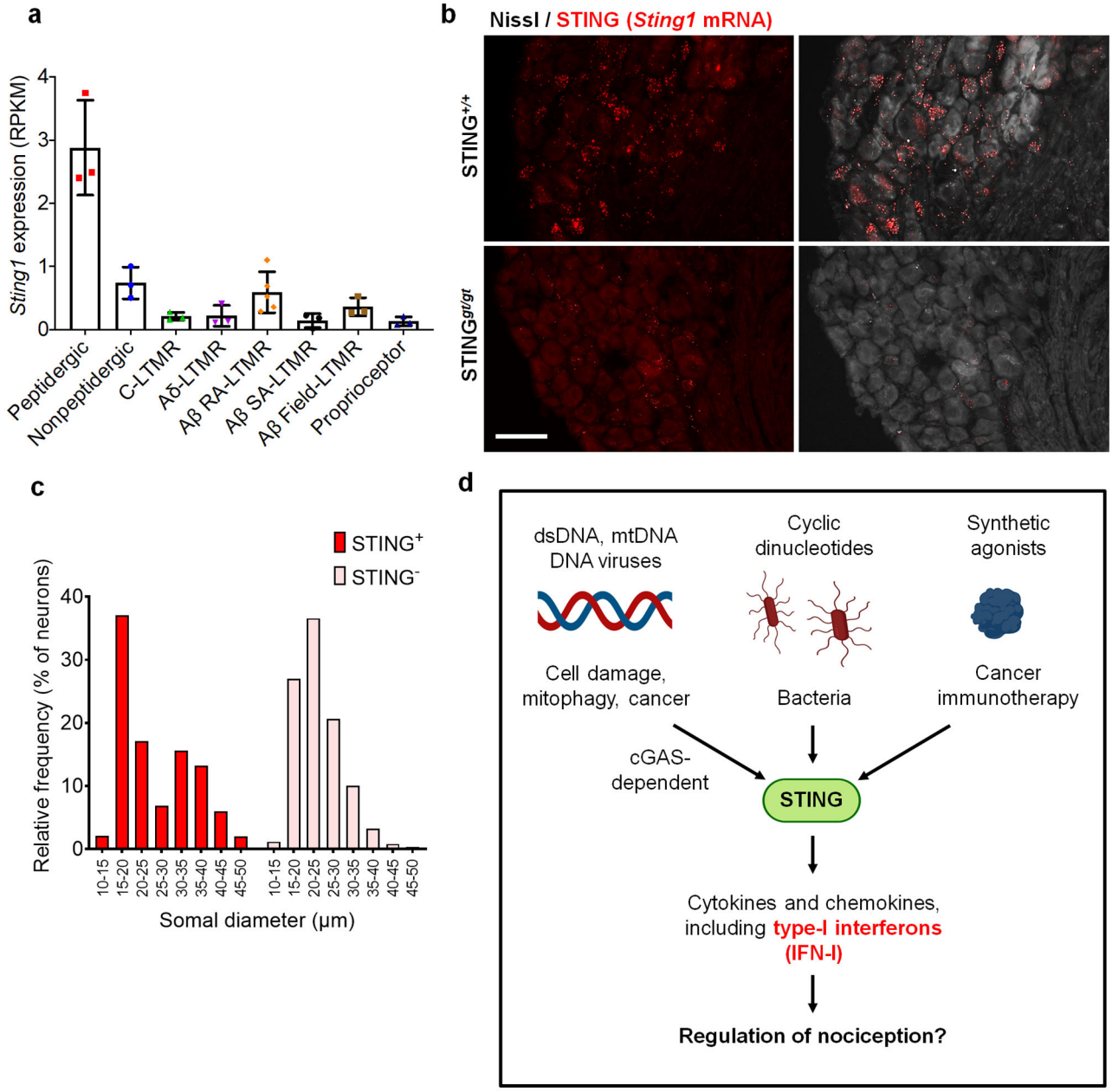

Extended Data Figure 1. STING is expressed in nociceptive sensory neurons in the DRG.

(**a**) *Sting1* (STING) mRNA expression in sensory neuron populations recently profiled and described by Zhang et al. (2019). Peptidergic nociceptive sensory neurons exhibit the highest expression of STING. **b-c**. *In situ* hybridization of *Sting1* in adult DRG sensory neurons using RNAscope, in conjunction with *Nissl* staining to label all neurons (**b**). STING expression is primarily observed in small-diameter sensory neurons. Quantification of DRG neurons expressing STING (≥5 puncta) or lacking STING found that approximately 60% of DRG neurons express STING. Scale bar is 100 μm. (**c**) Quantification of somal diameter in $STING^+$ and $STING^-$ neurons indicated that STING-expressing neurons are primarily

small-diameter sensory neurons. (**d**) Schematic indicating the various stimuli which activate STING and its downstream pathway. See Supplementary Table-1 for complete sample sizes, sex, and statistical information.

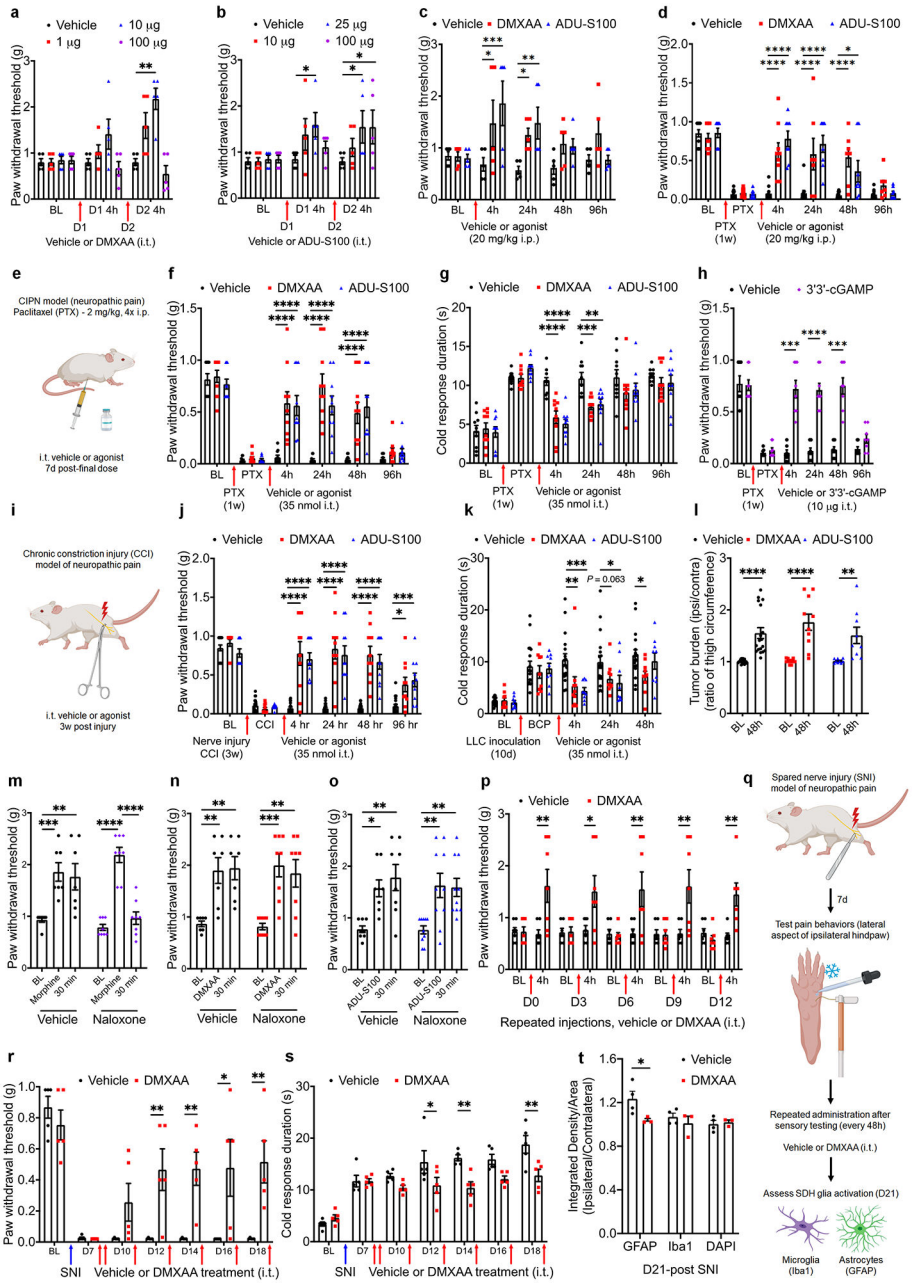

Extended Data Figure 2. Antinociceptive effects of STING agonists in naïve mice and in mouse models of neuropathic and cancer pain.

(**a**) Naïve mice were administered vehicle or the STING agonist DMXAA via i.t. injection (red arrows), followed by Von Frey testing to determine mechanical thresholds at 4h following the 1st (day 1, D1) or 2nd (D2) injection. STING agonists induced a dose-dependent increase in paw withdrawal thresholds, which was further amplified by multiple

injections. 10 μg (35 nmol) exhibited the largest effect, and therefore, was used throughout the rest of the study. (**b**) Naïve mice were administered vehicle or ADU-S100, a STING agonist with cross-species activity, via i.t. injection (red arrows) and tested as in panel a. 25 μg (35 nmol) exhibited the largest increase in paw withdrawal thresholds and this dose was used throughout the rest of the study. (**c**) Systemic administration of DMXAA and ADU-S100 increased paw withdrawal threshold in naïve mice for up to 24h. (**d**) In the CIPN model, i.p. DMXAA and ADU-S100 suppressed mechanical allodynia for up to 48h. Some toxicity was observed with systemic administration in the CIPN model, as 3 mice in the DMXAA group died 24h after the 2nd injection. No mice died in the vehicle or ADU-S100 groups. (**e**) A chemotherapy-induced peripheral neuropathy (CIPN) model of neuropathic pain was established with paclitaxel. **f-g**. In the CIPN model, i.t. DMXAA and ADU-S100 suppressed mechanical allodynia (**f**) and cold allodynia (**g**), as determined by response duration (in seconds) to acetone. (**h**) i.t. administration with the natural STING ligand 3'3'-cGAMP also reduced CIPN-induced mechanical allodynia. (**i**) STING agonists were also tested in the sciatic nerve chronic constriction injury (CCI) model of neuropathic pain. (**j**) i.t. treatment with DMXAA and ADU-S100 led to prolonged inhibition of mechanical allodynia (as determined by withdrawal threshold). **k-l.** Administration of DMXAA and ADU-S100 also suppressed cold allodynia (**k**) in the BCP model. These effects were not secondary to direct antitumor effects, as tumor burden was unaffected by STING agonist treatment (**l**). **m-o**. Effects of naloxone on morphine-, DMXAA-, and ADU-S100-induced antinociception. (**m**) Naloxone (10 mg/kg, i.p.) reversed morphine (2 nmol i.t.)-induced antinociception but had no effect on the antinociceptive effects of DMXAA (35 nmol, i.t.) (**n**) or ADU-S100 (35 nmol, i.t.) (**o**). (**p**) Repeated administration of DMXAA (35 nmol, i.t.) did not induce tolerance in naïve mice. **q-t**. Pain and glial reaction after spared nerve injury (SNI). (**q**) Paradigm of experimental design. Pain behaviors and spinal dorsal horn glial cell activation were assessed following repeated administration with vehicle or DMXAA (red arrows) in mice receiving SNI . Mechanical allodynia (**r**) and cold allodynia (**s**) were significantly reduced in DMXAA-treated mice at later timepoints (starting at D12). (**t**) Quantification of GFAP^{+} (astrocytes), Iba1^{+} (microglia), or DAPI (all cells) in the spinal dorsal horn (SDH) of mice at D21 after sustained vehicle or DMXAA treatment as indicated in panel o. SNI increased astrocyte activation (GFAP) in vehicle- but not DMXAA-treated mice. Values represent the ipsilateral (injured) SDH normalized to the contralateral (uninjured) SDH. All data are expressed as the mean ± s.e.m. * $P < 0.05$; ** $P < 0.01$; *** $P < 0.001$, **** $P < 0.0001$. Statistical comparisons were conducted with two-way ANOVA with Dunnett's (**a, b, c, d, f, g, k**), Sidak's (**h, j, l, s**), Bonferroni's (**m, n, o, p, r, t**), or Tukey's post-hoc test (**m, n, o**) See Supplementary Table-1 for complete sample sizes, sex, and statistical information.

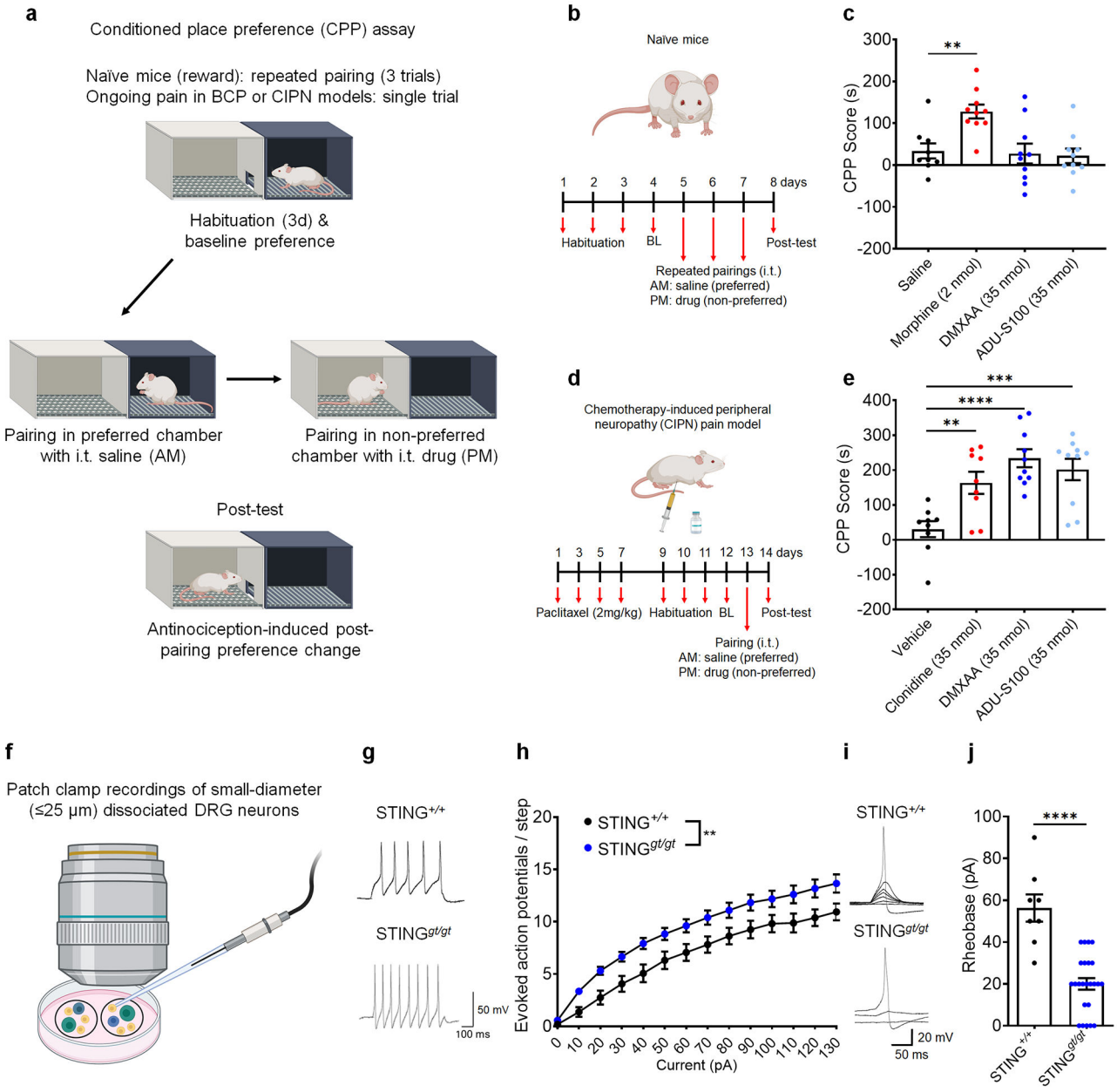

Extended Data Figure 3. STING agonists induce conditioned place preference in mice with neuropathic pain but not in naïve mice.

(**a**) Schematic indicating the experimental setup for the conditioned place preference (CPP) assay used to measure ongoing pain in mice. (**b**) Schematic indicating CPP protocol for naïve mice. CPP in naïve mice was performed using repeated pairings (3 trials). (**c**) Repeated pairing with i.t. morphine (2 nmol), but not DMXAA or ADU-S100 (35 nmol), induces CPP in naïve mice. (**d**) Schematic indicating CPP protocol for mice in the chemotherapy-induced peripheral neuropathy (CIPN) model of neuropathic pain. (**e**) A single pairing with i.t. DMXAA and ADU-S100 (35 nmol) induced comparable CPP as clonidine (35 nmol), a strong analgesic when administered via i.t. injection. **f**. Schematic depicting patch clamp recordings in small diameter dissociated DRG neurons from STING

$^{+/+}$ (WT) or STING$^{gt/gt}$ (gKO) mice. (**g-h**) STING$^{gt/gt}$ mice exhibit increased excitability, as determined by number of action potentials evoked per current step (in 10 pA increments). (**i-j**) Nociceptors from STING$^{gt/gt}$ mice also exhibit decreased rheobase at baseline. All data are expressed as the mean ± s.e.m. * $P < 0.05$; ** $P < 0.01$; *** $P < 0.001$, **** $P < 0.0001$. Statistical comparisons were conducted with one-way ANOVA with Fisher's LSD test (**c, e**), two-way ANOVA with Bonferroni's post-hoc test (**h**), or two-tailed t-test (**j**). See Supplementary Table-1 for complete sample sizes, sex, and statistical information.

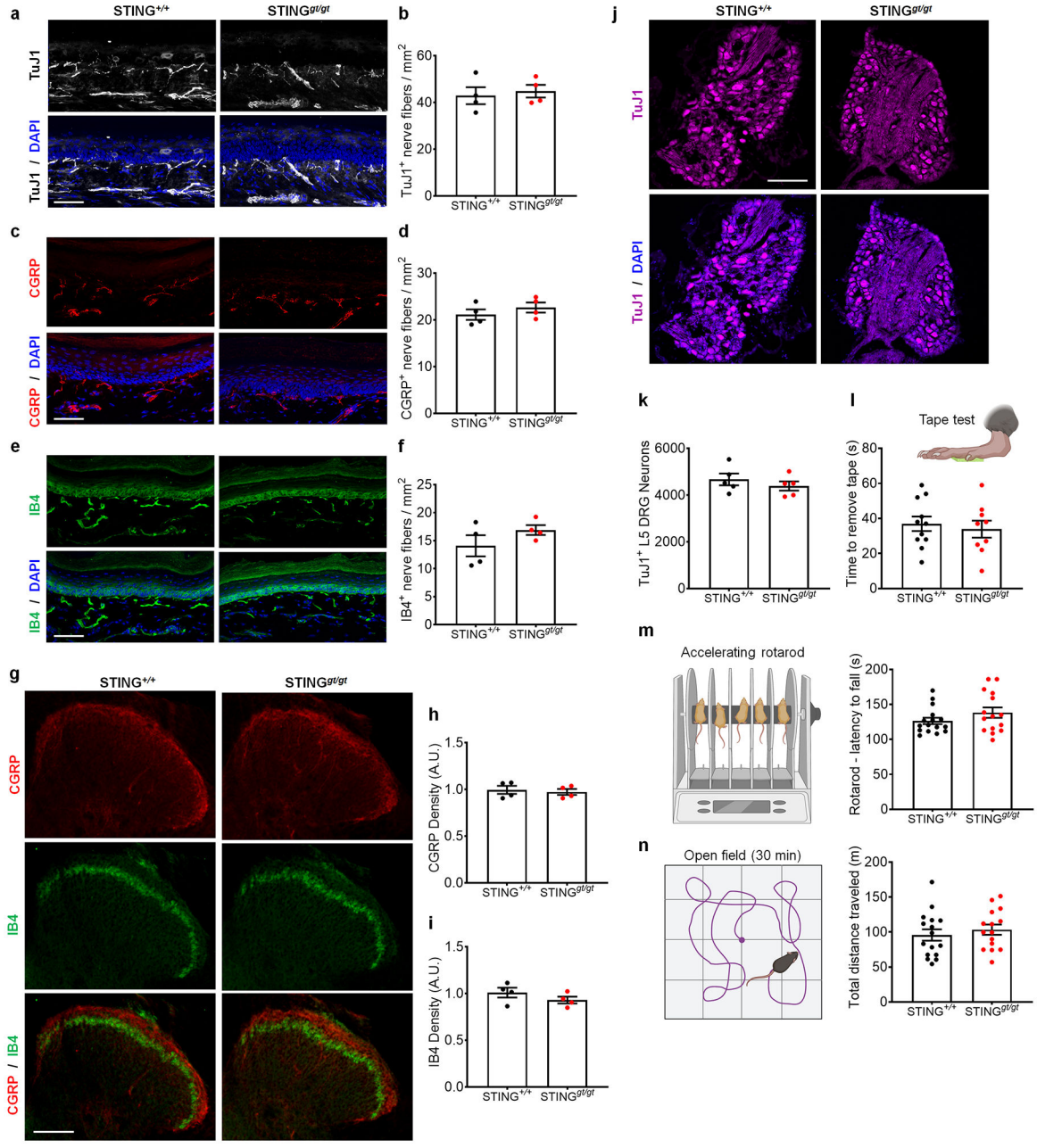

Extended Data Figure 4. Mice lacking STING exhibit normal innervation patterns, sensory neuron numbers, and sensorimotor behaviors.

a-f. Hindpaw skin immunostaining for nerve fibers (a, c, e) and their quantification (b, d, f) from STING$^{+/+}$ or STING$^{gt/gt}$ mice. (**a**) TuJ1 to label all nerve fibers, (**c**) CGRP to label fibers from peptidergic nociceptors, or (**e**) IB4 to label fibers from nonpeptidergic nociceptors. In each case, sections were counterstained with DAPI to identify the dermis-epidermis junction. Quantification of (**b**) TuJ1^{+}, (**d**) CGRP^{+}, and (**f**) IB4^{+} nerve fibers indicate that STING-WT and -gKO mice have similar peripheral innervation densities. Scale bar for (**a-f**) is 50 μm. **g-i**. L3-L5 spinal cord segments were collected from STING$^{+/+}$ and STING$^{gt/gt}$ mice and immunostained for CGRP (red) and IB4 (green) to label central nociceptive terminals. (**g**) Representative images, scale bar is 100 μm. Image J quantification of (**h**) CGRP and (**i**) IB4 pixel density in the spinal dorsal horn (displayed in arbitrary units, A.U.) indicates that there are no changes in central innervation density in STING$^{gt/gt}$ mice. **j-k**. Analysis of total DRG neuron numbers in STING$^{+/+}$ and STING$^{gt/gt}$ mice. (**j**) L5 DRGs were collected from STING$^{+/+}$ and STING$^{gt/gt}$ mice, serially sectioned at 14 μm, and every 3rd section was immunostained for the pan-neuronal marker TuJ1 (purple), counterstained with DAPI (blue). Scale bar is 200 μm. (**k**) Quantification of total DRG neuron numbers indicated that STING$^{+/+}$ and STING$^{gt/gt}$ have similar sensory neuron numbers. **l-n**. No differences were observed between STING$^{+/+}$ and STING$^{gt/gt}$ mice in the (**l**) tape test, a measure of sensorimotor function, (**m**) in an accelerating rotarod test to measure motor function, or (**n**) in locomotor activity in the open field test (30 min test duration). All data are expressed as the mean ± s.e.m. * $P < 0.05$; ** $P < 0.01$; *** $P < 0.001$, **** $P < 0.0001$. Statistical comparisons were conducted with two-tailed t-test. See Supplementary Table-1 for complete sample sizes, sex, and statistical information.

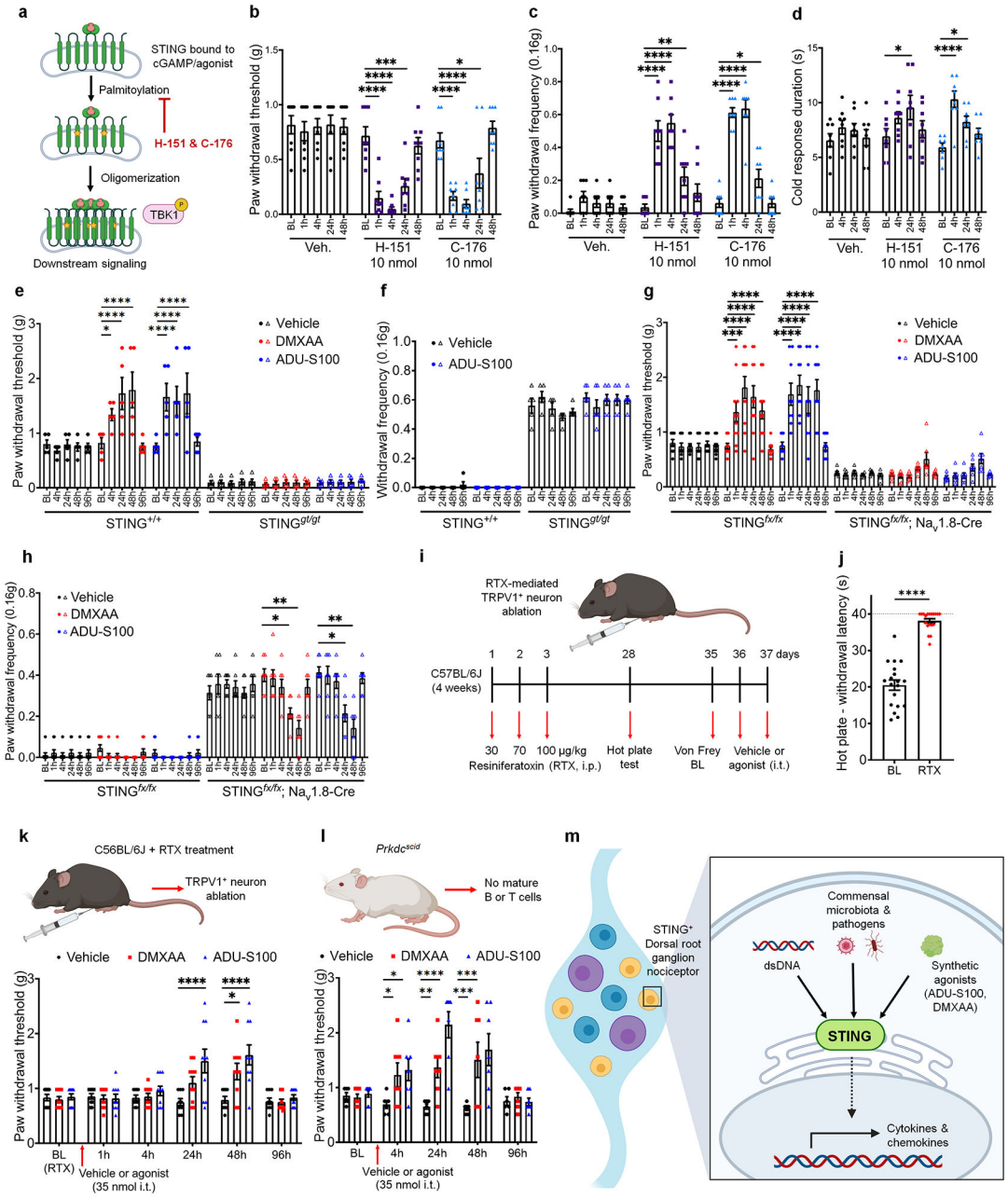

Extended Data Figure 5. STING signaling in nociceptors is required for the antinociceptive effects of STING agonists.

(**a**) Schematic showing mechanism of action of the small molecule STING inhibitors H-151 and C-176. (**b-d**) i.t. administration of H-151 and C-176 induced transient mechanical (**b-c**) and cold hypersensitivity (**d**) in naïve mice. (**e**) DMXAA and ADU-S100 (35 nmol each, i.t.) increased paw withdrawal thresholds in STING$^{+/+}$ but not in STING$^{gt/gt}$ mice. (**f**). Administration of ADU-S100 (35 nmol, i.t.) did not alter paw withdrawal frequency to a low-threshold 0.16g Von Frey filament in STING$^{gt/gt}$ mice. (**g**) DMXAA and ADU-S100 increased paw withdrawal threshold in STING$^{fx/fx}$ (WT) mice, but no significant effects were observed in STING$^{fx/fx}$; Na$_v$1.8-Cre mice. A non-statistically significant increase in

withdrawal thresholds was observed at later timepoints (24h, 48h) in STING$^{fx/fx}$; $Na_v1.8$-Cre mice. (**h**) DMXAA and ADU-S100 (35 nmol each, i.t.) reduced mechanical hypersensitivity (determined by withdrawal frequency to a 0.16g Von Frey filament) in STING$^{fx/fx}$; $Na_v1.8$-Cre mice at 24h and 48h. (**i**) Schematic indicating method of resiniferatoxin (RTX) treatment and the effects of STING agonists in RTX-treated mice. (**j**) RTX increased withdrawal latency in the hotplate test (cutoff time = 40s). (**k**) The early (1h, 4h, 24h) antinociceptive effects of DMXAA and ADU-S100 (35 nmol, i.t.) were abolished by RTX. (**l**) The antinociceptive effects of DMXAA and ADU-S100 (35 nmol, i.t.) showed a normal time course of effects (relative to Fig. 1b) in *Prkdc*^{scid} mice, which lack mature B and T cells. (**m**) Schematic indicating possible upstream activators of STING in sensory neurons, and proposed mechanism by which STING$^+$ neurons regulate nociception through induction of cytokines and chemokines. While our data support that STING signaling in nociceptors contributes to the early antinociceptive effects of STING agonists, additional cell types including other sensory neuron populations and peripheral immune cells may also contribute to the prolonged antinociceptive effects at later timepoints. All data are expressed as the mean ± s.e.m. * $P < 0.05$; ** $P < 0.01$; *** $P < 0.001$, **** $P < 0.0001$. Statistical comparisons were conducted with two-way ANOVA with Dunnett's (vs. BL; **b, c, d, e, f, g, h**) or Tukey's (**k, l**) post-hoc tests. Comparisons between two groups (**j**) were conducted with two-tailed t-test. See Supplementary Table-1 for complete sample sizes, sex, and statistical information.

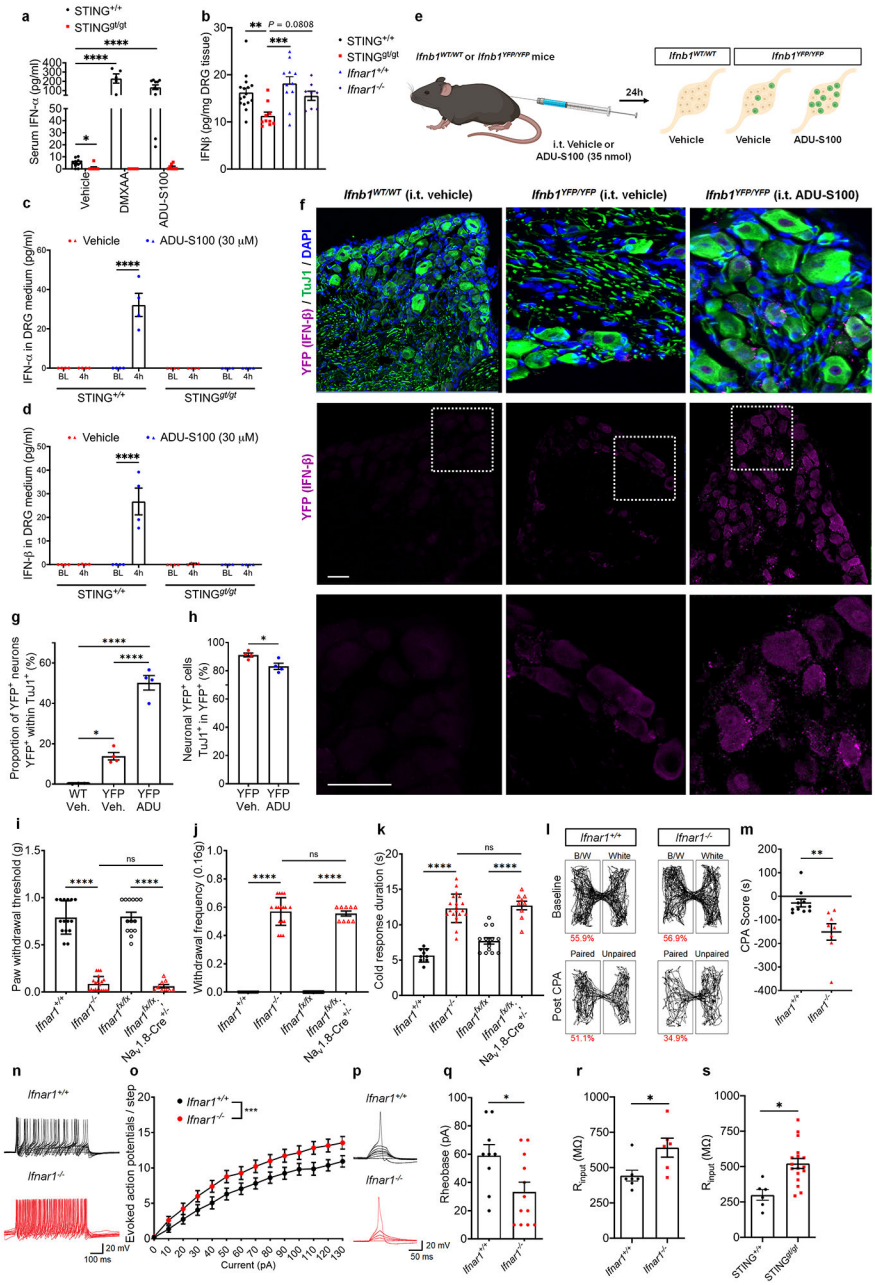

Extended Data Figure 6. STING agonists induce IFN-I production in sensory neurons *in vitro* and *in vivo*.

(**a**) Intrathecal administration of STING agonists increases IFN-α in serum 24h following injection in WT, but not STING$^{gt/gt}$ mice. (**b**) While basal IFN-β could be detected in DRG tissue from all genotypes, STING$^{gt/gt}$ mice exhibited significantly lower IFN-β levels. **c-d**. ADU-S100 treatment of high density DRG neuron cultures from STING$^{+/+}$ or STING$^{gt/gt}$ mice. In WT DRG neurons, ADU-S100 induced release of IFN-α (**c**) and IFN-β (**d**) into the culture medium, determined by ELISA. **e-h**. IFN-β expression in mouse DRG neurons. (**e**) Schematic showing experimental design to determine which cell types within the DRG produce IFN-β in response to i.t. STING activation with ADU-S100 using an *Ifnb1*^{YFP}

reporter mouse. (**f-h**) Administration of ADU-S100 induced an increase in YFP expression (indicating IFN-β expressing cells) within the DRG. (**f**) Representative images showing YFP (purple), TuJ1 (green), and DAPI (blue). Scale bar is 50 μm. (**g**) ADU-S100 increased the proportion of total neurons expressing YFP^+ in *Ifnb1*$^{YFP/YFP}$ mice; virtually no YFP^+ cells detected in WT *Ifnb1*$^{+/+}$ mice. (**h**) YFP expression was primarily detected in $TuJ1^+$ neurons rather than $TuJ1^-$ non-neuronal cell types, although this neuronal expression bias was reduced by ADU-S100 treatment. **i-k** Mice lacking *Ifnar1* globally (*Ifnar1*$^{-/-}$) or selectively in sensory neurons (*Ifnar1*$^{fx/fx}$; $Na_v1.8$-Cre) exhibit significantly increased sensitivity to mechanical stimuli determined by (**i**) paw withdrawal threshold or (**j**) paw withdrawal frequency to a low stimulus 0.16g Von Frey filament, compared to their littermate controls. (**k**) These mice also exhibit increased sensitivity to cold stimulation. **l-m**. CPA testing was performed as in Fig. 1l. Pairing in the preferred chamber with 0.04g filament induced CPA in *Ifnar1*$^{-/-}$ mice, but not *Ifnar1*$^{+/+}$ littermate control mice. (**l**) Representative trackplots of mouse movement pre- and post-pairing. (**m**) Quantification of CPA score (Pre – post, in seconds). **n-q**. Action potentials (**n-o**) and rheobases (**p-q**) in DRG nociceptors as in Figure 2g-j. *Ifnar1*$^{-/-}$ mice exhibit increased excitability, as determined by (**n-o**) number of action potentials evoked per current step (in 10 pA increments) or (**p-q**) basal rheobase. **r-s**. Input resistance was calculated from patch clamp recordings from DRG nociceptors from mice of the indicated genotypes. Increased input resistance was observed in neurons from both *Ifnar1*$^{-/-}$ (**r**) and STING$^{gt/gt}$ (**s**) mice compared to their WT littermates. All data are expressed as the mean ± s.e.m. * $P < 0.05$; ** $P < 0.01$; *** $P < 0.001$, **** $P < 0.0001$. Statistical comparisons were conducted with one-way ANOVA with Tukey's post-hoc test (**b, g, i, j, k**) two-way ANOVA with Dunnett's post-hoc test (**a, c, d, o**), or two-tailed t-test (**h, m, q, r, s**). See Supplementary Table-1 for complete sample sizes, sex, and statistical information.

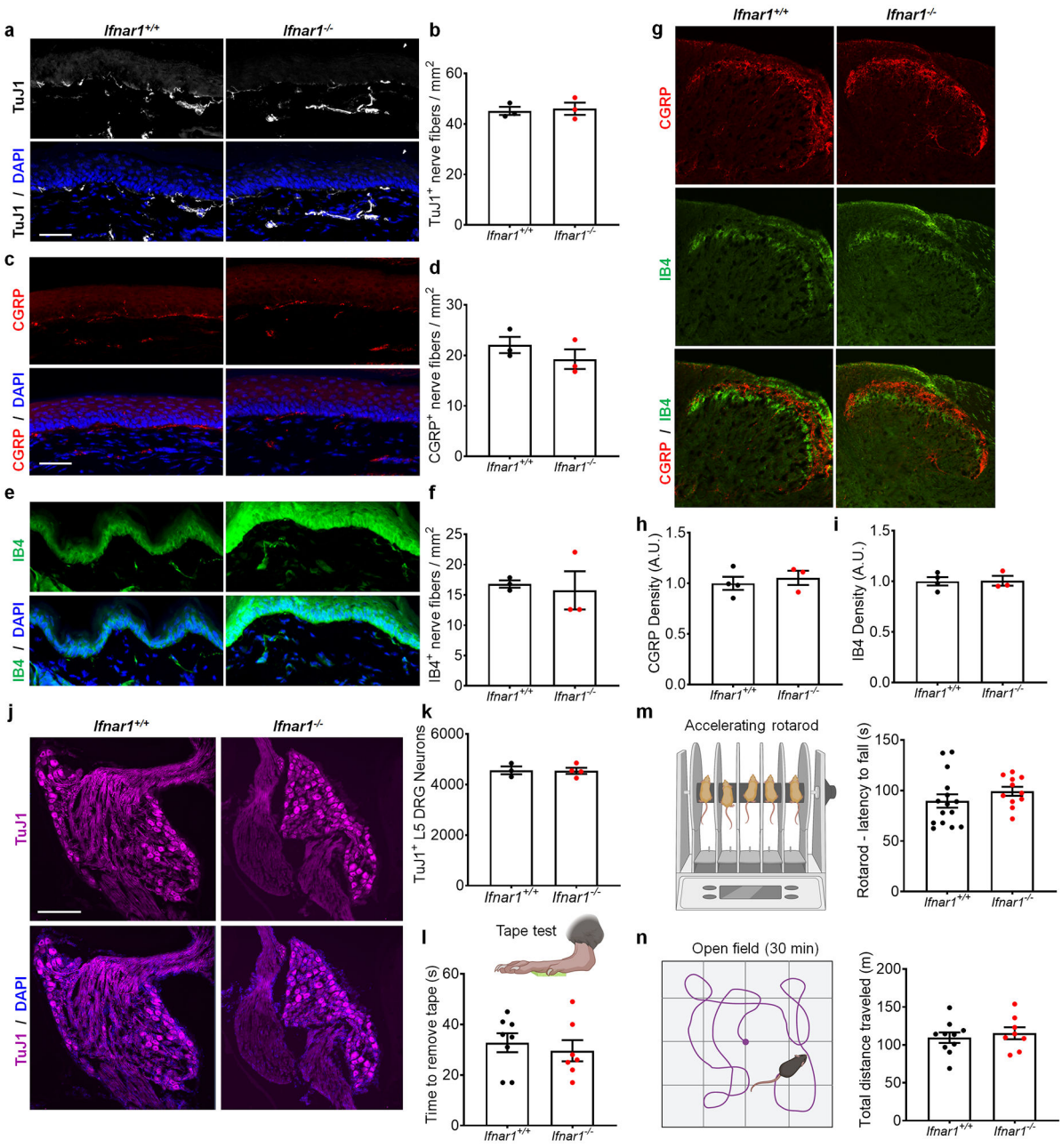

Extended Data Figure 7. Mice lacking *Ifnar1* exhibit normal innervation patterns, sensory neuron numbers, and sensorimotor behaviors.

a-f. Hindpaw skin was collected from *Ifnar1*$^{+/+}$ or *Ifnar1*$^{-/-}$ mice and immunostained for (**a**) TuJ1, (**c**) CGRP, or (**e**) IB4 with DAPI as in Extended Data Fig. 4. Quantification of epidermal (**b**) TuJ1^{+}, (**d**) CGRP^{+}, and (**f**) IB4^{+} nerve fibers indicate that similar skin innervation densities for each marker in WT and KO mice. Scale bar for (**a-f**) is 50 μm. **g-i**. L3-L5 spinal cord segments were collected from *Ifnar1*$^{+/+}$ or *Ifnar1*$^{-/-}$ mice and immunostained for CGRP (red) and IB4 (green) to label central nociceptive terminals in the dorsal horn. (**g**) Representative images, scale bar is 100 μm. Image J quantification of (**h**) CGRP and (**i**) IB4 pixel density (displayed in arbitrary units, A.U.) indicates similar

densities of central innervation. **j-k**. (**j**) L5 DRGs were collected from *Ifnar1*$^{+/+}$ and *Ifnar1*$^{-/-}$ mice and total cell counts were performed as in Extended Data Fig. 4 using TuJ1 (purple) and DAPI (blue). Scale bar is 200 μm. (**k**) Quantification of total DRG neuron numbers indicated that *Ifnar1*$^{+/+}$ or *Ifnar1*$^{-/-}$ mice have similar numbers of L5 DRG neurons. **l-n**. No differences were observed between *Ifnar1*$^{+/+}$ and *Ifnar1*$^{-/-}$ mice in the (**l**) tape test, (**m**) in the accelerating rotarod test, or (**n**) in locomotor activity in the open field test (30 minute duration). All data are expressed as the mean ± s.e.m. * $P < 0.05$; ** $P < 0.01$; *** $P < 0.001$, **** $P < 0.0001$. Statistical comparisons were conducted with two-tailed t-test. See Supplementary Table-1 for complete sample sizes, sex, and statistical information.

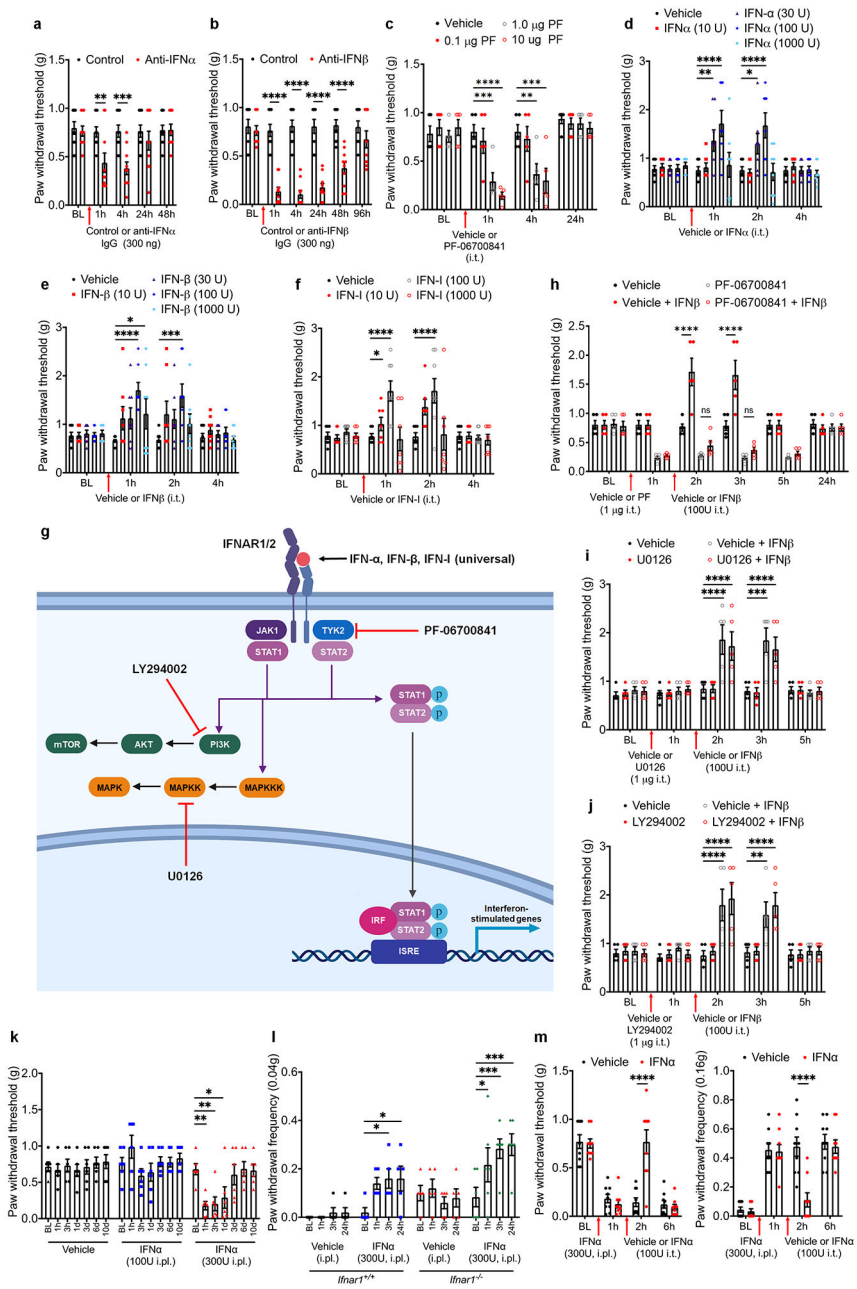

Extended Data Figure 8. Type-I interferons regulate nociception in mice via Tyk2.

a-b. Inhibition of endogenous IFN-I signaling via i.t. administration of (**a**) an anti-IFN-α neutralizing antibody or (**b**) an anti-IFN-β neutralizing antibody (vs. IgG control, 300 ng) induced transient mechanical allodynia in naïve mice. (**c**) Inhibition of the IFN-I signaling adapter Tyk2 with PF-06700841 (i.t., 1 μ) induced transient, dose-dependent mechanical allodynia in naïve mice. **d-f**. i.t. injection of recombinant (**d**) murine IFN-α, (**e**) murine IFN-β (produced in mammalian cells), or (**f**) universal IFN-I increased paw withdrawal thresholds in naïve mice. Notably, 100 U exhibited the greatest effects for each recombinant ligand. At higher concentrations some mice exhibited mechanical hypersensitivity. (**g**) Schematic showing downstream IFN-I signaling pathways and the pharmacologic inhibitors

used to target Tyk2, PI3K, or MAPKK. **h**. Pretreatment of naïve mice with the Tyk2 inhibitor PF-06700841 (i.t., 1μg) abolished IFN-β-induced antinociception. **i-j**. Pre-treatment with (**i**) 1 μg i.t. U0126, a MAPKK (MEK) inhibitor or (**j**) 1 μg LY294002, a PI3K inhibitor, failed to affect IFN-β-induced increased paw withdrawal threshold. (**k**) Intraplantar (i.pl., e.g. hindpaw) administration of IFN-α at high concentrations induced prolonged mechanical hypersensitivity. (**l**), i.pl. injection of 300U IFN-α evokes mechanical hypersensitivity in both WT and *Ifnar1*$^{-/-}$ mice, as determined by paw withdrawal frequency to repeated stimulation with a very low threshold Von Frey filament (0.04g, selected due to the baseline hypersensitivity of *Ifnar1*$^{-/-}$ mice). (**m**) Mechanical hypersensitivity induced by i.pl. injection of 300U IFN-α is attenuated by i.t. IFN-α administration, as determined by paw withdrawal threshold (left panel) or withdrawal frequency (right panel) to repeated stimulation with 0.16g Von Frey filament. All data are expressed as the mean ± s.e.m. * $P < 0.05$; ** $P < 0.01$; *** $P < 0.001$, **** $P < 0.0001$. Statistical comparisons were conducted with two-way ANOVA with Bonferroni's (**a, b, m**) or Dunnett's post-hoc test (**c, d, e, f, h, i, j, k, l**). See Supplementary Table-1 for complete sample sizes, sex, and statistical information.

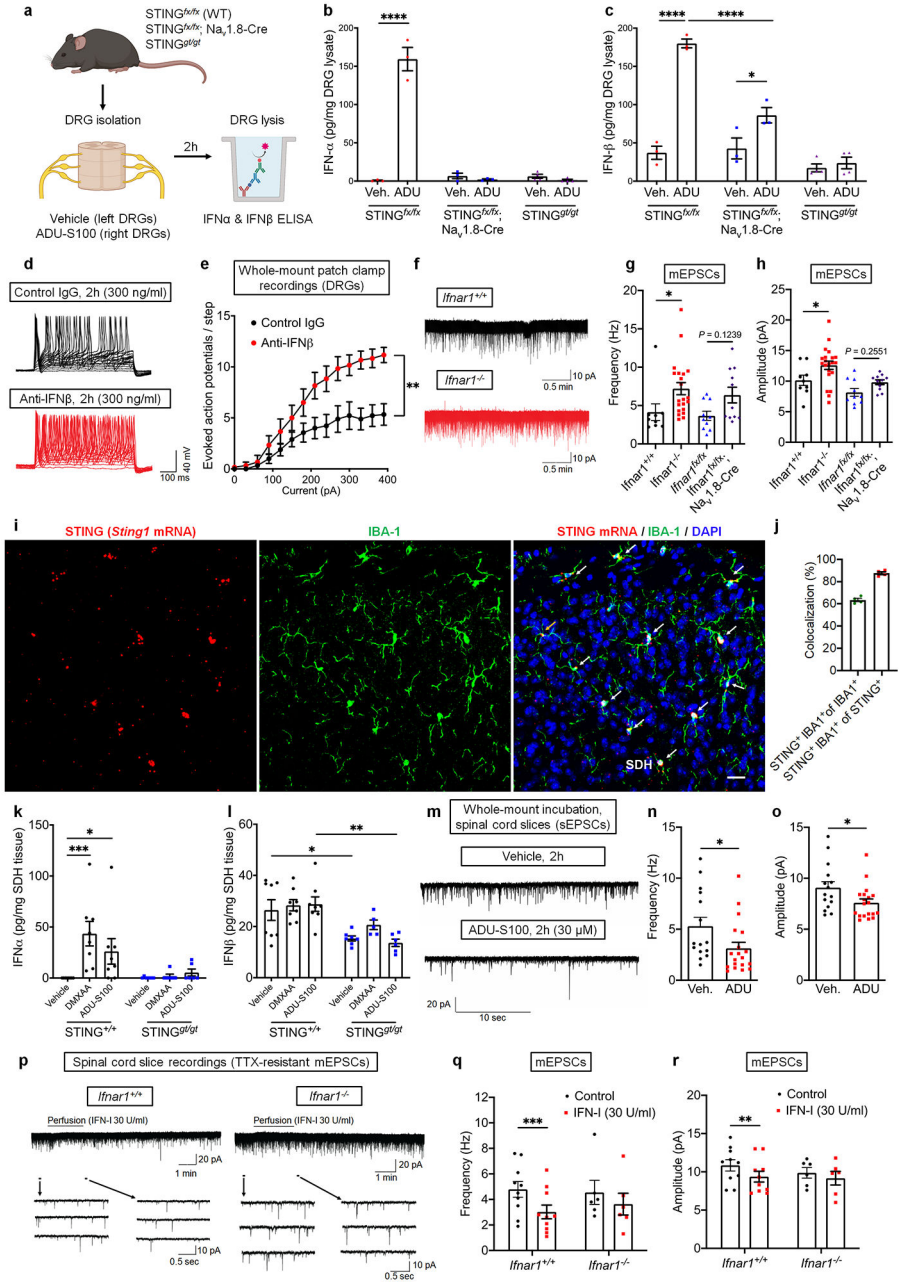

Extended Data Figure 9. Peripheral and central actions of STING-mediated IFN-I signaling in DRG and spinal cord.

(**a**) L1-L5 DRGs were isolated from STING$^{fx/fx}$, STING$^{fx/fx}$; $Na_v1.8$-Cre, and STING$^{gt/gt}$ mice and incubated *ex vivo* with vehicle (left DRGs) or 30 μM ADU-S100 (right DRGs) for 2h, followed by lysis and IFN-α and IFN-β ELISA. (**b**) IFN-α and (**c**) IFN-β levels in DRG lysate were increased by *ex vivo* incubation with ADU-S100 in WT mice. ADU-S100 induced a significant elevation of IFN-β in STING$^{fx/fx}$; $Na_v1.8$-Cre DRG lysate, but this increase was significantly lower than that seen in WT mice. **d-e**. DRGs from naïve mice were incubated *ex vivo* in control IgG or anti-IFNβ for 2h followed by whole-mount patch clamp recordings from DRG nociceptors. (**d**) Representative traces and (**e**) quantification of

current-evoked action potentials. Anti-IFNβ treatment significantly increased action potential firing. **f-h**. Recordings of miniature EPSCs (mEPSCs) from outer lamina II spinal dorsal horn neurons in spinal cord slices from mice of the indicated genotypes. (**f**) Representative traces and quantification of mEPSC (**g**) frequency and (**h**) amplitude. *Ifnar1*$^{-/-}$ mice exhibit increased frequency and amplitude compared to WT littermates. No significant increase was observed in *Ifnar1*$^{fx/fx}$; $Na_v1.8$-Cre mice relative to *Ifnar1*$^{fx/fx}$ controls. (**i**) Representative images of RNAscope showing *Sting1* (STING) mRNA (red) in conjunction with Iba1 immunostaining to label microglia (green) in the spinal cord dorsal horn (SDH). Yellow arrows indicate STING^{+}/Iba1^{+} cells. Scale bar represents 20 μm. (**j**) Quantification indicates that STING is predominantly expressed by microglia in the SDH. (**k**) IFN-α and (**l**) IFN-β levels in SDH lysate in mice of the indicated genotypes 24h after STING agonist administration showing induction of IFN-α but not IFN-β. Basal IFN-β production was significantly lower in STING$^{gt/gt}$ mice. **m-o**. *Ex vivo* incubation of spinal cord slices from naïve mice with ADU-S100. (**m**) Representative traces and quantification of (**n**) frequency and (**o**) amplitude of spontaneous EPSCs (sEPSCs) from outer lamina II spinal dorsal horn neurons. ADU-S100 significantly reduced the frequency and amplitude of sEPSCs. **p-r**. Acute perfusion of spinal cord slices with IFN-I and recording of TTX-resistant mEPSCs from outer lamina II spinal dorsal horn neurons. (**p**) Representative traces from *Ifnar1*$^{+/+}$ and *Ifnar1*$^{-/-}$ mice, with IFN-I perfused as indicated and the areas indicated by the black bars magnified for enhanced resolution. Quantification of (**q**) frequency and (**r**) amplitude of mEPSC in neurons from WT and KO mice pre- and 1 min post- perfusion with IFN-I. Acute IFN-I treatment significantly reduced the frequency and amplitude of mEPSCs in WT mice. All data are expressed as the mean ± s.e.m. * $P < 0.05$; ** $P < 0.01$; *** $P < 0.001$, **** $P < 0.0001$. Statistical comparisons were conducted with one-way or two-way ANOVA with Sidak's (**b, c, g, h**) or Bonferroni post-hoc test (**e, k, l, q, r**) or two-tailed t-test (**n, o**). See Supplementary Table-1 for complete sample sizes, sex, and statistical information.

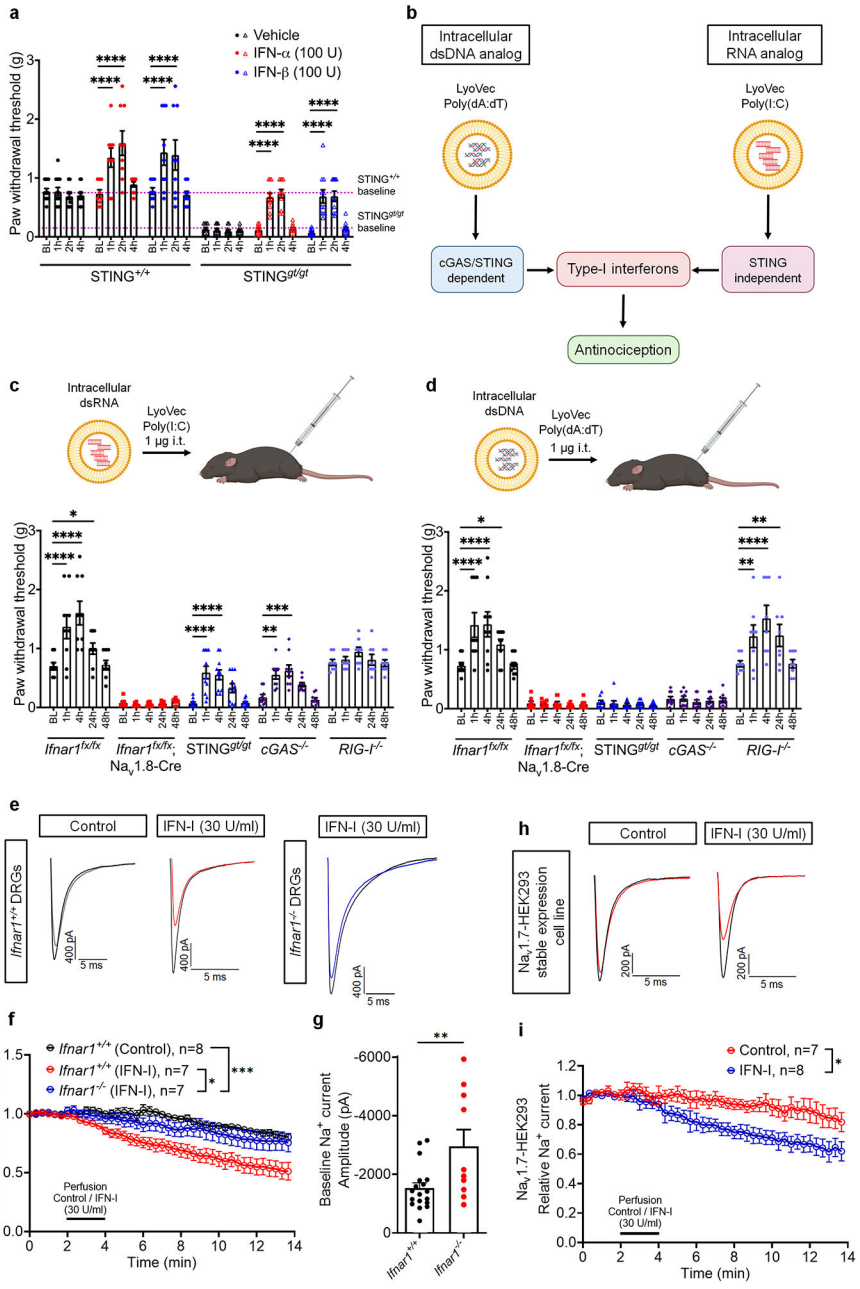

Extended Data Figure 10. dsDNA induces antinociception via the cGAS/STING/IFN-I pathway and proposed mechanism of STING/IFN-I regulation of nociception.

(**a**) i.t. IFN-α and IFN-β elevated mechanical thresholds in WT mice and could transiently rescue the mechanical hypersensitivity phenotype of STING$^{gt/gt}$ mice back to levels comparable to WT baseline levels. (**b**) Schematic illustrating intracellular poly(dA:dT) induces cGAS/STING-dependent IFN-I upregulation whereas intracellular poly(I:C) induces IFN-I response through a STING-independent mechanism. **c-d**. Mice of the indicated genotypes were administered 1 μg poly(I:C) or 1 μg poly(dA:dT) via i.t. injection followed by Von Frey testing to determine mechanical thresholds at the indicated timepoints. (**c**) i.t. poly(I:C) elevated mechanical thresholds in *Ifnar1*$^{fx/fx}$ (WT), STING$^{gt/gt}$, and *cGAS*$^{-/-}$

mice, but these effects were abolished in *Ifnar1*$^{fx/fx}$;Na_v1.8-Cre and *RIG-I*$^{-/-}$ mice. (**d**) i.t. poly(dA:dT) elevated mechanical thresholds in WT and *RIG-I*$^{-/-}$ mice, but these effects were abolished in *Ifnar1*$^{fx/fx}$;Na_v1.8-Cre, STING$^{gt/gt}$, and *cGAS*$^{-/-}$ mice. **e-g**. Sodium currents were recorded from DRG nociceptors cultured from *Ifnar1*$^{+/+}$ or *Ifnar1*$^{-/-}$ mice, perfused with vehicle or IFN-I for 2 minutes as indicated. (**e**) Representative traces and (**f**) quantification of Na^+ currents demonstrating that rIFN-I treatment led to a reduction in sodium currents. (**g**) Nociceptors from *Ifnar1*-gKO mice exhibited increased Na^+ current amplitude at baseline. **h-i**. HEK293 cells stably expressing the voltage-gated sodium channel Na_v1.7 were perfused as in panel f and Na^+ currents were recorded. (**h**) Representative traces and (**i**) Timecourse of Na_v1.7-mediated currents. IFN-I perfusion reduced Na_v1.7-mediated currents.

All data are expressed as the mean ± s.e.m. * $P < 0.05$; ** $P < 0.01$; *** $P < 0.001$, **** $P < 0.0001$. Statistical comparisons were conducted with two-way ANOVA with Dunnett's post-hoc test (**a, c, d**), two-way ANOVA with Bonferroni's post-hoc test (**f, i**), or two-tailed t-test (**g**). See Supplementary Table-1 for complete sample sizes, sex, and statistical information.

Supplementary Material

Refer to Web version on PubMed Central for supplementary material.

Acknowledgements

We thank J. P.-Y. Ting and B. D. X. Lascelles for helpful discussions and R. Kuner for providing Nav1.8-cre mice. This study was supported by Duke University Anesthesiology research funds and Duke Microbiome Center fund granted to R.-R.J. C.R.D. was also supported by the International Association for the Study of Pain John J. Bonica Trainee Fellowship, NIH T32 training grant GM008600, and the Department of Anesthesiology, Duke University. M.-C.K. and the monkey study was supported by NIH R21 grant DA044450.

Data availability statement:

The data will be available upon request. Ru-Rong Ji (ru-rong.ji@duke.edu) and Christopher R. Donnelly (christopher.donnelly@duke.edu).

References

1. Ishikawa H & Barber GN STING is an endoplasmic reticulum adaptor that facilitates innate immune signalling. Nature 455, 674–678, doi:10.1038/nature07317 (2008). [PubMed: 18724357]
2. Woo SR et al. STING-dependent cytosolic DNA sensing mediates innate immune recognition of immunogenic tumors. Immunity 41, 830–842, doi:10.1016/j.immuni.2014.10.017 (2014). [PubMed: 25517615]
3. Kwon J & Bakhoum SF The Cytosolic DNA-Sensing cGAS-STING Pathway in Cancer. Cancer Discov 10, 26–39, doi:10.1158/2159-8290.Cd-19-0761 (2020). [PubMed: 31852718]
4. Julius D & Basbaum AI Molecular mechanisms of nociception. Nature 413, 203–210 (2001). [PubMed: 11557989]
5. Donnelly CR, Chen O & Ji RR How Do Sensory Neurons Sense Danger Signals? Trends Neurosci, doi:10.1016/j.tins.2020.07.008 (2020).
6. Sneddon LU Comparative Physiology of Nociception and Pain. Physiology (Bethesda) 33, 63–73, doi:10.1152/physiol.00022.2017 (2018). [PubMed: 29212893]
7. Baral P, Udit S & Chiu IM Pain and immunity: implications for host defence. Nature reviews. Immunology 19, 433–447, doi:10.1038/s41577-019-0147-2 (2019).

8. Ji RR, Chamessian A & Zhang YQ Pain regulation by non-neuronal cells and inflammation. Science 354, 572–577, doi:10.1126/science.aaf8924 (2016). [PubMed: 27811267]
9. Zheng Y et al. Deep Sequencing of Somatosensory Neurons Reveals Molecular Determinants of Intrinsic Physiological Properties. Neuron, doi:10.1016/j.neuron.2019.05.039 (2019).
10. Yaksh TL & Rudy TA Analgesia mediated by a direct spinal action of narcotics. Science 192, 1357–1358 (1976). [PubMed: 1273597]
11. Costigan M, Scholz J & Woolf CJ Neuropathic pain: a maladaptive response of the nervous system to damage. Annu.Rev.Neurosci. 32, 1–32, doi:10.1146/annurev.neuro.051508.135531 [doi] (2009). [PubMed: 19400724]
12. Wang K et al. PD-1 blockade inhibits osteoclast formation and murine bone cancer pain. The Journal of clinical investigation 130, 3603–3620, doi:10.1172/jci133334 (2020). [PubMed: 32484460]
13. Mogil JS Animal models of pain: progress and challenges. Nat.Rev.Neurosci 10, 283–294, doi:nrn2606 [pii];10.1038/nrn2606 [doi] (2009). [PubMed: 19259101]
14. Navratilova E & Porreca F Reward and motivation in pain and pain relief. Nature neuroscience 17, 1304–1312, doi:10.1038/nn.3811 (2014). [PubMed: 25254980]
15. Ji RR, Donnelly CR & Nedergaard M Astrocytes in chronic pain and itch. Nature reviews. Neuroscience 20, 667–685, doi:10.1038/s41583-019-0218-1 (2019). [PubMed: 31537912]
16. Hummel M, Lu P, Cummons TA & Whiteside GT The persistence of a long-term negative affective state following the induction of either acute or chronic pain. Pain 140, 436–445, doi:10.1016/j.pain.2008.09.020 (2008). [PubMed: 18945547]
17. Agarwal N, Offermanns S & Kuner R Conditional gene deletion in primary nociceptive neurons of trigeminal ganglia and dorsal root ganglia. Genesis. 38, 122–129, doi:10.1002/gene.20010 [doi] (2004). [PubMed: 15048809]
18. Haag SM et al. Targeting STING with covalent small-molecule inhibitors. Nature 559, 269–273, doi:10.1038/s41586-018-0287-8 (2018). [PubMed: 29973723]
19. Usoskin D et al. Unbiased classification of sensory neuron types by large-scale single-cell RNA sequencing. Nat.Neurosci 18, 145–153, doi:nn.3881 [pii];10.1038/nn.3881 [doi] (2015). [PubMed: 25420068]
20. Fensome A et al. Dual Inhibition of TYK2 and JAK1 for the Treatment of Autoimmune Diseases: Discovery of ((S)-2,2-Difluorocyclopropyl)((1 R,5 S)-3-(2-((1-methyl-1 H-pyrazol-4-yl)amino)pyrimidin-4-yl)-3,8-diazabicyclo[3.2.1]octan-8-yl)methanone (PF-06700841). Journal of medicinal chemistry 61, 8597–8612, doi:10.1021/acs.jmedchem.8b00917 (2018). [PubMed: 30113844]
21. Harari D et al. Enhanced in vivo efficacy of a type I interferon superagonist with extended plasma half-life in a mouse model of multiple sclerosis. The Journal of biological chemistry 289, 29014–29029, doi:10.1074/jbc.M114.602474 (2014). [PubMed: 25193661]
22. Barragán-Iglesias P et al. Type I Interferons Act Directly on Nociceptors to Produce Pain Sensitization: Implications for Viral Infection-Induced Pain. J Neurosci 40, 3517–3532, doi:10.1523/jneurosci.3055-19.2020 (2020). [PubMed: 32245829]
23. Todd AJ Neuronal circuitry for pain processing in the dorsal horn. Nature reviews. Neuroscience 11, 823–836, doi:10.1038/nrn2947 (2010). [PubMed: 21068766]
24. Sun L, Wu J, Du F, Chen X & Chen ZJ Cyclic GMP-AMP synthase is a cytosolic DNA sensor that activates the type I interferon pathway. Science 339, 786–791, doi:10.1126/science.1232458 (2013). [PubMed: 23258413]
25. Ivashkiv LB & Donlin LT Regulation of type I interferon responses. Nature reviews. Immunology 14, 36–49, doi:10.1038/nri3581 (2014).
26. Binshtok AM, Bean BP & Woolf CJ Inhibition of nociceptors by TRPV1-mediated entry of impermeant sodium channel blockers. Nature 449, 607–610, doi:nature06191 [pii];10.1038/nature06191 [doi] (2007). [PubMed: 17914397]
27. Hu E, Calo G, Guerrini R & Ko MC Long-lasting antinociceptive spinal effects in primates of the novel nociceptin/orphanin FQ receptor agonist UFP-112. Pain 148, 107–113, doi:10.1016/j.pain.2009.10.026 (2010). [PubMed: 19945794]

28. Sjostrom S, Tamsen A, Persson MP & Hartvig P Pharmacokinetics of intrathecal morphine and meperidine in humans. Anesthesiology 67, 889–895, doi:10.1097/00000542-198712000-00003 (1987). [PubMed: 2891329]
29. Crow MK, Olferiev M & Kirou KA Type I Interferons in Autoimmune Disease. Annual review of pathology 14, 369–393, doi:10.1146/annurev-pathol-020117-043952 (2019).
30. Neufeld NJ, Elnahal SM & Alvarez RH Cancer pain: a review of epidemiology, clinical quality and value impact. Future oncology (London, England) 13, 833–841, doi:10.2217/fon-2016-0423 (2017).
31. Sivick KE et al. Magnitude of Therapeutic STING Activation Determines CD8(+) T Cell-Mediated Anti-tumor Immunity. Cell Rep 25, 3074–3085.e3075, doi:10.1016/j.celrep.2018.11.047 (2018). [PubMed: 30540940]
32. Tan YS et al. Mitigating SOX2-potentiated Immune Escape of Head and Neck Squamous Cell Carcinoma with a STING-inducing Nanosatellite Vaccine. Clin Cancer Res 24, 4242–4255, doi:10.1158/1078-0432.Ccr-17-2807 (2018). [PubMed: 29769207]
33. Scheu S, Dresing P & Locksley RM Visualization of IFNbeta production by plasmacytoid versus conventional dendritic cells under specific stimulation conditions in vivo. Proceedings of the National Academy of Sciences of the United States of America 105, 20416–20421, doi:10.1073/pnas.0808537105 (2008). [PubMed: 19088190]
34. Sauer JD et al. The N-ethyl-N-nitrosourea-induced Goldenticket mouse mutant reveals an essential function of Sting in the in vivo interferon response to Listeria monocytogenes and cyclic dinucleotides. Infection and immunity 79, 688–694, doi:10.1128/iai.00999-10 (2011). [PubMed: 21098106]
35. Jin L et al. MPYS is required for IFN response factor 3 activation and type I IFN production in the response of cultured phagocytes to bacterial second messengers cyclic-di-AMP and cyclic-di-GMP. Journal of immunology (Baltimore, Md. : 1950) 187, 2595–2601, doi:10.4049/jimmunol.1100088 (2011).
36. Prigge JR et al. Type I IFNs Act upon Hematopoietic Progenitors To Protect and Maintain Hematopoiesis during Pneumocystis Lung Infection in Mice. Journal of immunology (Baltimore, Md. : 1950) 195, 5347–5357, doi:10.4049/jimmunol.1501553 (2015).
37. Schoggins JW et al. Pan-viral specificity of IFN-induced genes reveals new roles for cGAS in innate immunity. Nature 505, 691–695, doi:10.1038/nature12862 (2014). [PubMed: 24284630]
38. Agarwal N, Offermanns S & Kuner R Conditional gene deletion in primary nociceptive neurons of trigeminal ganglia and dorsal root ganglia. Genesis. 38, 122–129, doi:10.1002/gene.20010 [doi] (2004). [PubMed: 15048809]
39. Sisignano M et al. Targeting CYP2J to reduce paclitaxel-induced peripheral neuropathic pain. Proceedings of the National Academy of Sciences of the United States of America 113, 12544–12549, doi:10.1073/pnas.1613246113 (2016). [PubMed: 27791151]
40. Chen G et al. PD-L1 inhibits acute and chronic pain by suppressing nociceptive neuron activity via PD-1. Nature neuroscience 20, 917–926, doi:10.1038/nn.4571 (2017). [PubMed: 28530662]
41. Decosterd I & Woolf CJ Spared nerve injury: an animal model of persistent peripheral neuropathic pain. Pain 87, 149–158 (2000). [PubMed: 10924808]
42. Chaplan SR, Bach FW, Pogrel JW, Chung JM & Yaksh TL Quantitative assessment of tactile allodynia in the rat paw. J.Neurosci Methods 53, 55–63 (1994). [PubMed: 7990513]
43. Chen G, Park CK, Xie RG & Ji RR Intrathecal bone marrow stromal cells inhibit neuropathic pain via TGF-beta secretion. J Clin.Invest 125, 3226–3240, doi:80883 [pii];10.1172/JCI80883 [doi] (2015). [PubMed: 26168219]
44. Bouet V et al. The adhesive removal test: a sensitive method to assess sensorimotor deficits in mice. Nature protocols 4, 1560–1564, doi:10.1038/nprot.2009.125 (2009). [PubMed: 19798088]
45. King T et al. Unmasking the tonic-aversive state in neuropathic pain. Nat.Neurosci. 12, 1364–1366, doi:nn.2407 [pii];10.1038/nn.2407 [doi] (2009). [PubMed: 19783992]
46. Zhang Z et al. Persistent pain facilitates response to morphine reward by downregulation of central amygdala GABAergic function. Neuropsychopharmacology : official publication of the American College of Neuropsychopharmacology 39, 2263–2271, doi:10.1038/npp.2014.77 (2014). [PubMed: 24686896]

47. Hummel M, Lu P, Cummons TA & Whiteside GT The persistence of a long-term negative affective state following the induction of either acute or chronic pain. Pain 140, 436–445, doi:10.1016/j.pain.2008.09.020 (2008). [PubMed: 18945547]

48. Ren BX et al. Intrathecal injection of metabotropic glutamate receptor subtype 3 and 5 agonist/antagonist attenuates bone cancer pain by inhibition of spinal astrocyte activation in a mouse model. Anesthesiology 116, 122–132, doi:10.1097/ALN.0b013e31823de68d (2012). [PubMed: 22123524]

49. Haag SM et al. Targeting STING with covalent small-molecule inhibitors. Nature 559, 269–273, doi:10.1038/s41586-018-0287-8 (2018). [PubMed: 29973723]

50. Demaria O et al. STING activation of tumor endothelial cells initiates spontaneous and therapeutic antitumor immunity. Proceedings of the National Academy of Sciences of the United States of America 112, 15408–15413, doi:10.1073/pnas.1512832112 (2015). [PubMed: 26607445]

51. Xu ZZ et al. Inhibition of mechanical allodynia in neuropathic pain by TLR5-mediated A-fiber blockade. Nature medicine 21, 1326–1331, doi:10.1038/nm.3978 (2015).

52. Wang Z et al. Anti-PD-1 treatment impairs opioid antinociception in rodents and nonhuman primates. Sci Transl Med 12, doi:10.1126/scitranslmed.aaw6471 (2020).

53. Jiang C et al. PD-1 Regulates GABAergic Neurotransmission and GABA-Mediated Analgesia and Anesthesia. iScience 23, 101570, doi:10.1016/j.isci.2020.101570 (2020). [PubMed: 33083737]

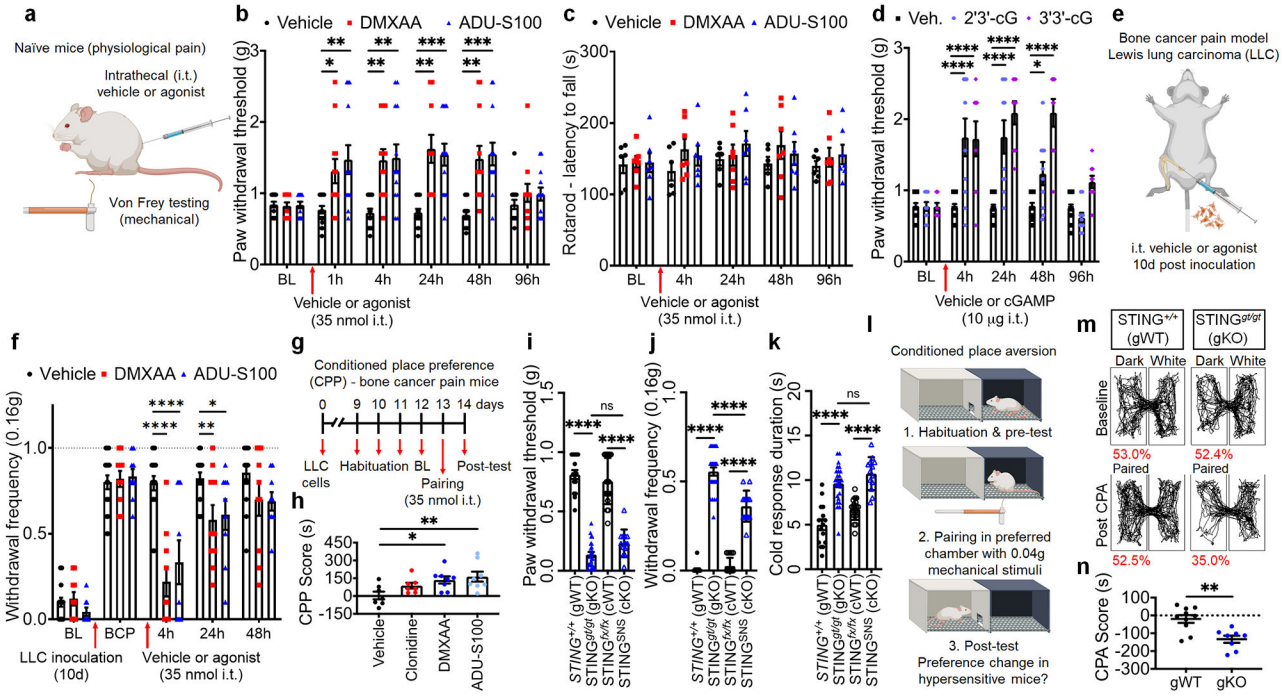

Figure 1. STING inhibits nociception in naïve and injured mice

a-c. Naïve mice were administered vehicle or STING agonists via intrathecal (i.t., **a**) injection for two successive days, followed by von Frey testing at the indicated timepoints. (**b**) STING agonists elevated mechanical thresholds for up to 48h. (**c**) STING agonists did not affect motor function in rotarod test. (**d**) i.t. injection of the natural STING ligands 2'3'-cGAMP and 3'3'-cGAMP elevated mechanical thresholds in naïve mice. **e-f**. A syngeneic bone cancer pain model (BCP) was established, followed by i.t. vehicle or STING agonist 10d post-inoculation. STING agonists suppressed BCP-induced mechanical allodynia. (**g**) Experimental layout to test whether i.t. STING agonists can suppress ongoing pain in the BCP model using a conditioned place preference (CPP) assay. (**h**) CPP was observed in STING agonist-paired mice compared to vehicle-paired mice. **i-k**. Compared to their corresponding wildtype (WT) littermates, STING$^{gt/gt}$ and STING$^{fx/fx}$; $Na_v1.8$-Cre mice exhibit increased sensitivity to (**i**, **j**) mechanical stimuli, and (**k**) cold stimuli. (**l**) A conditioned place aversion (CPA) assay was used to assess hypersensitivity to mechanical stimulation using repeated stimulation with an innocuous 0.04g Von Frey filament. (**m**) Representative track plots in WT and STING$^{gt/gt}$ mice. (**n**) Quantification of CPA score. All data are expressed as the mean ± s.e.m. * $P < 0.05$; ** $P < 0.01$; *** $P < 0.001$, **** $P < 0.0001$. Statistical comparisons were conducted with two-way ANOVA with Dunnett's post-hoc test (vehicle vs. agonist; **b-f**) or Tukey's post-hoc test (**i-k**), one-way ANOVA with Fisher's LSD post-hoc test (vehicle-paired vs. drug-paired; **h**), or two-tailed t-test (**n**). See Supplementary Table-1 for complete sample sizes, sex, and statistical information.

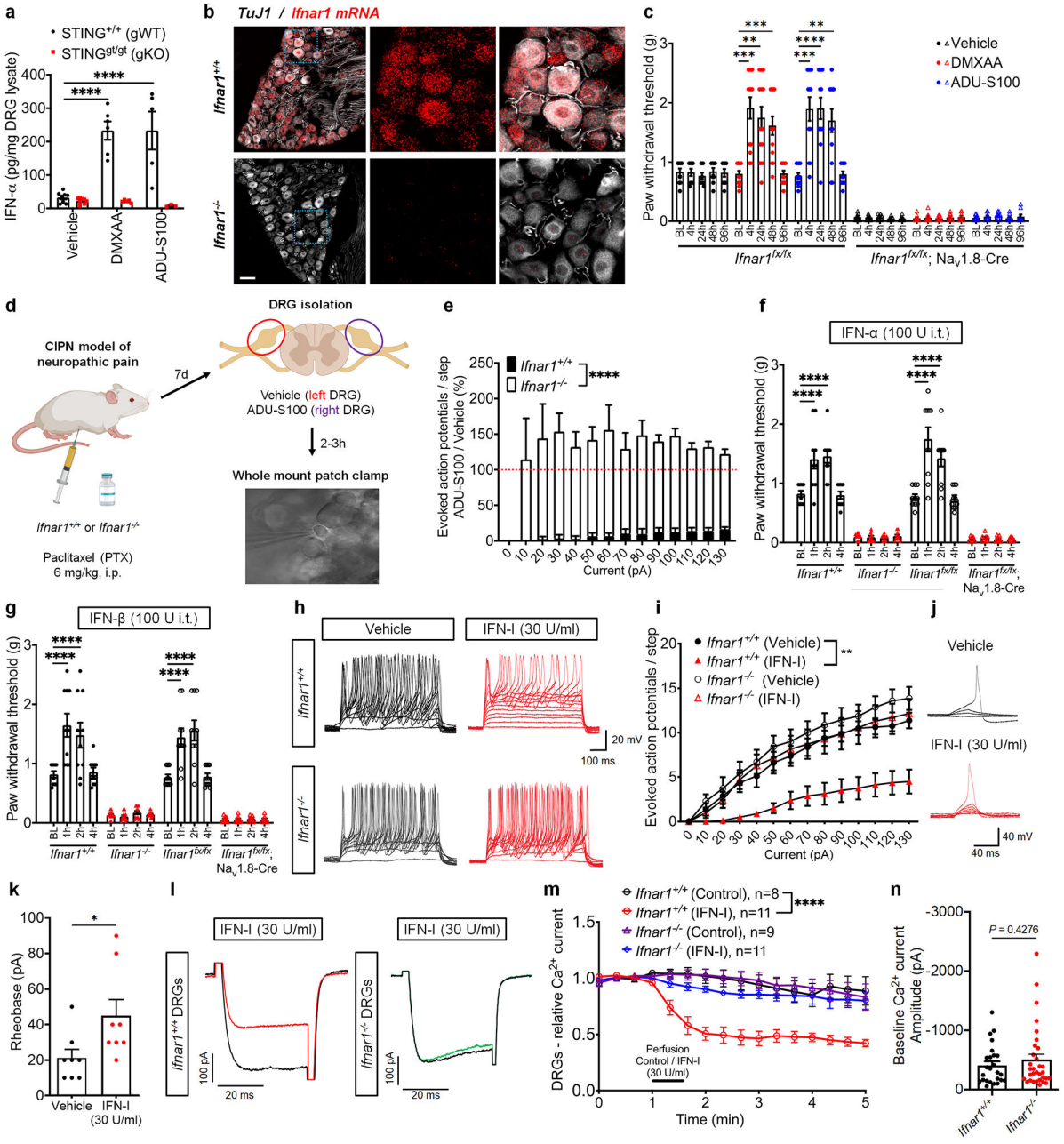

Figure 2. STING inhibits nociception via type-I interferon signaling in nociceptors.

(**a**) Intrathecal administration of STING agonists increased IFN-α in DRG lysate 24h following injection in WT, but not STING$^{gt/gt}$ mice. (**b**) *Ifnar1 in situ* hybridization (red) in conjunction with immunostaining for the pan-neuronal marker TuJ1 (white) indicates that *Ifnar1* is expressed by virtually all DRG neurons in naïve mice. (**c**) STING agonists elevated mechanical thresholds in *Ifnar1*$^{fx/fx}$ (WT) but not *Ifnar1*$^{fx/fx}$; $Na_v1.8$-Cre (cKO) mice. (**d**) Schematic of experimental design for whole-mount patch clamp experiments in DRGs. (**e**) Current-evoked action potentials were recorded, and the percent change by ADU-S100 (relative to vehicle) in *Ifnar1*$^{+/+}$ (WT; black bars) or *Ifnar1*$^{-/-}$ DRGs (gKO; white bars) is displayed (red line indicates no change). ADU-S100 led to a sharp reduction in DRG

excitability in WT but not gKO DRGs. (**f**) IFN-α and (**g**) IFN-β each induced transient antinociception in WT mice which was abolished in *Ifnar1*-gKO/cKO mice. **h-i**. Patch clamp recordings in dissociated DRG neurons from *Ifnar1*$^{+/+}$ or *Ifnar1*$^{-/-}$ mice after acute perfusion with vehicle or rIFN-I. (**h**) Representative traces and (**i**) quantification of current evoked action potentials. IFN-I inhibited action potential firing in DRG neurons from WT, but not gKO mice. (**j-k**) rIFN-I treatment also increased rheobase in WT neurons, with representative traces (j) and quantification (k) indicated. (**l**) Representative traces and (**m**) quantification of Ca^{2+} currents. rIFN-I perfusion decreased Ca^{2+} currents in nociceptors from WT but not *Ifnar1*-gKO mice. (**n**) Amplitude of Ca^{2+} currents at baseline in nociceptors from WT and *Ifnar1*-gKO mice. All data are expressed as the mean ± s.e.m. * $P < 0.05$; ** $P < 0.01$; *** $P < 0.001$, **** $P < 0.0001$. Statistical comparisons were conducted with two-way ANOVA with Bonferroni's (**e, i, m**) or Dunnett's post-hoc test (**a, c, f, g**, relative to BL within each group), or two-tailed t-test (*k, n*). See Supplementary Table-1 for complete sample sizes, sex, and statistical information.

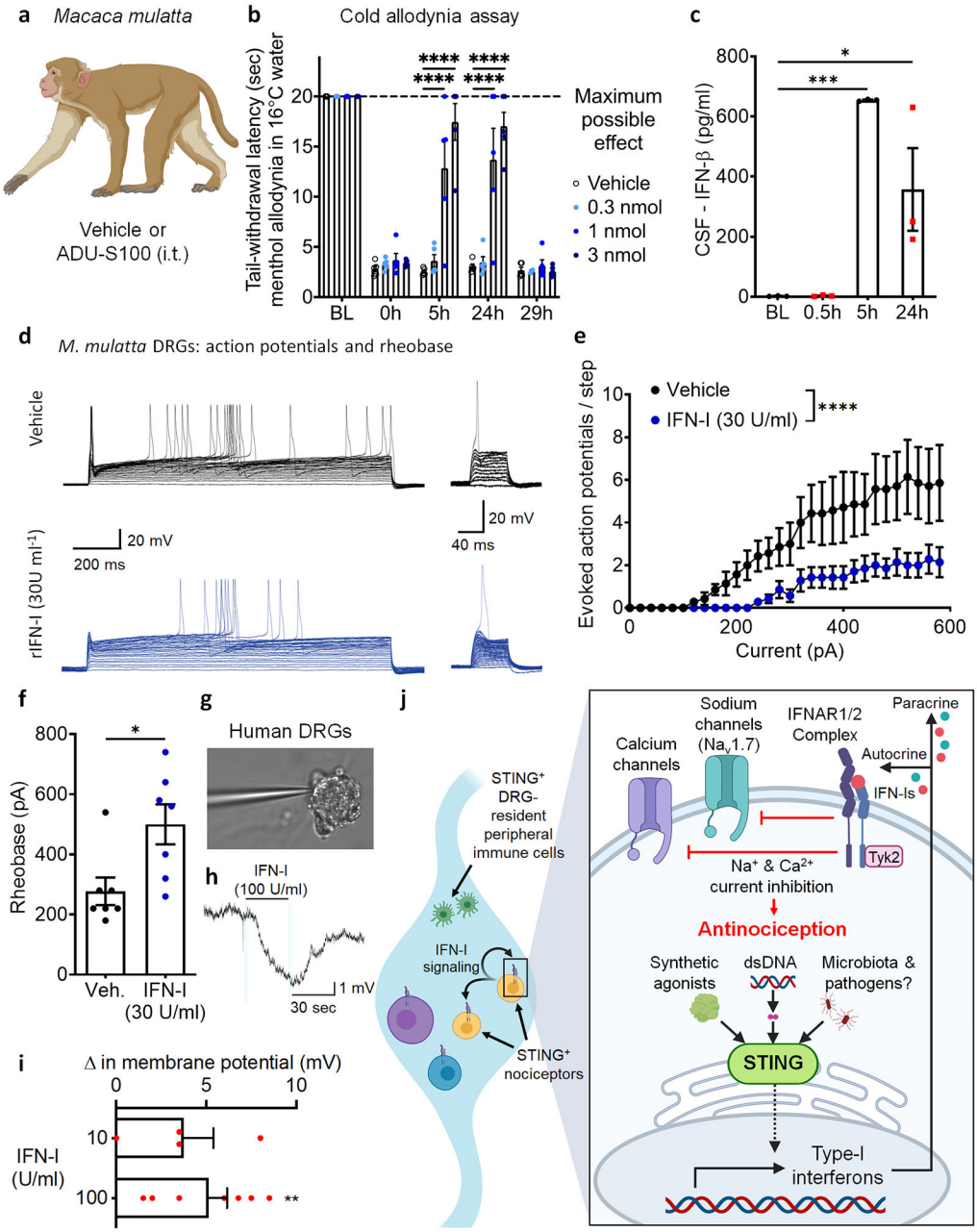

Figure 3. STING-mediated IFN-I signaling suppresses pain and nociceptor excitability in non-human primates and humans.

a-c Administration of ADU-S100 via i.t. catheter in non-human primates (*Macaca mulatta*, **a**) (**b**) attenuated 2% menthol gel-induced cold allodynia in a dose-dependent manner, and (**c**) increased IFN-β in cerebrospinal fluid (CSF) in NHPs treated with 3 nmol ADU-S100. **d-f**. Patch clamp recordings on DRG nociceptors from NHPs acutely treated with vehicle or rIFN-I as in Fig. 2h. (**d**) Representative traces of current evoked action potentials (left) and rheobase (right). (**e**) quantification of action potentials and (**f**) rheobase. rIFN-I perfusion inhibited NHP nociceptor excitability, as evidenced by reduced action potential firing and increased rheobase. **g-i**. Patch clamp recordings on small-diameter (< 55 μm) human DRG

neurons (hDRGs). (**g**) hDRG neuron with pipette attached for patch clamp recordings. (**h**) Representative recording following acute application of rIFN-I, which led to hyperpolarization of the membrane potential, quantified in (**i**). (**j**) Mechanisms by which autocrine and/or paracrine STING-mediated IFN-I signaling suppresses nociception. All data are expressed as the mean ± s.e.m. * $P < 0.05$; ** $P < 0.01$; *** $P < 0.001$, **** $P < 0.0001$. Statistical comparisons were conducted with two-way ANOVA with Dunnett's post-hoc test (**b, e**), one-way ANOVA with Dunnett's post-hoc test (**c**), two-tailed t-test (**f**), or one-sample t-test (vs. hypothetical value of 0). See Supplementary Table-1 for complete sample sizes, sex, and statistical information.